

A complete sample of LSP blazars fully described in γ -rays

New γ -ray detections and associations with Fermi-LAT

B. Arsioli^{1,2,3} and G. Polenta⁴

¹ Science Data Center della Agenzia Spaziale Italiana, SSDC - ASI, Rome, Italy

² Instituto de Física Gleb Wataghin, UNICAMP, R. Sérgio Buarque de Holanda 777, 13083-859 Campinas, Brazil

³ ICRANet-Rio, CBPF, Rua Dr. Xavier Sigaud 150, 22290-180 Rio de Janeiro, Brazil

⁴ ASI - Agenzia Spaziale Italiana, via del Politecnico snc, 00133 Roma, Italy

e-mail: bruno.arsioli@ssdc.asi.it, arsioli@ifgw.unicamp.br e-mail: gianluca.polenta@asi.it

Preprint online version: February 24, 2022

ABSTRACT

Context. We study the γ -ray and broadband spectral energy distribution (SED) properties of a complete sample of 104 bright, radio-selected low-synchrotron peaked (LSP) blazars, which have well-characterized SEDs from radio to X-rays. Most of the sources have already been detected in the γ -ray band by Fermi-LAT, however almost 20% of these blazars have no counterpart in any of the Fermi catalogs published so far.

Aims. Using the Fermi Science Tools, we look for γ -ray emission for those objects not yet reported in any Fermi-LAT catalog, finding new detections and associations. We then study the multifrequency SED for all sources in our sample, fitting their synchrotron (Syn) and inverse Compton (IC) components. A complete sample of LSP blazars with a full description in γ -ray is unique. We use this sample to derive the distribution of the Compton dominance (CD) along with population properties such as Syn and IC peak power, and frequency distributions.

Methods. We performed a binned likelihood analysis in the 0.3-500 GeV energy band with Fermi-LAT Pass 8 data, integrating over 7.5 years of observations. We studied γ -ray light curves and test statistic (TS) maps to validate new detections and associations, thereby building a better picture of the high-energy activity in radio-selected LSP blazars. We fit the IC component for the new detections using all data at our disposal from X-rays to GeV γ -rays, enhancing the amount of information available to study the Syn to IC peak-power correlations.

Results. We deliver a unique characterization in γ -rays for a complete sample of LSP blazars. We show that three previously unidentified 3FGL sources can be associated with blazars when using improved γ -ray positions obtained from TS maps. Six previously unreported γ -ray sources are detected at TS > 20 level, while another three show TS values between 10-20. We evaluate two cases in which source confusion is likely present. In four cases there is no significant γ -ray signature when integrating over 7.5 years. Short-lived flares at ~ 1 month scale, however, have been detected in these sources. Finally, we measure the log(CD) for the sample, which has a Gaussian-like distribution with median log(CD) ≈ 0.1 , implying that on average the peak-power for the Syn and IC components in LSP blazars are similar.

Key words. Gamma rays: Galaxies – Galaxies: Active – Radiation mechanism: Non-thermal

1. Introduction

Blazars are a particular class of jetted active galactic nuclei (AGN), corresponding to the very few cases where jets are pointing close to our line of sight (Padovani et al. 2017). These objects are known for having a rather unique spectral energy distribution (SED) often characterized by the presence of two nonthermal bumps in the $\log(\nu f_\nu)$ versus $\log(\nu)$ plane, which extends along the whole electromagnetic window from radio up to TeV γ -rays. Also known for their rapid and large amplitude spectral variability, usually the observed radiation shows extreme properties owing to the relativistic nature of the jets, which result in amplification effects. Blazars are relatively rare; there are ~ 4000 optically identified objects in the latest blazar surveys, 5BZcat (Massaro et al. 2015) and 2WHSP (Chang et al. 2017), and they have been extensively studied by means of a multifrequency approach.

According to the standard picture (e.g., Giommi et al. 2012a), the first peak in $\log(\nu f_\nu)$ vs. $\log(\nu)$ plane is associated with the emission of Syn radiation owing to relativistic electrons moving through the magnetic field of the collimated jet. The second peak is usually understood as a result of inverse Compton (IC) scattering of low energy photons to the highest energies, by the same relativistic electron population that generates these Syn photons (synchrotron self Compton model; SSC). The seed photons undergoing IC scattering can also come from outside regions, such as the accretion disk and broad line region, and can add an extra ingredient (external Compton models; EC) for modeling the observed SED.

Since the peak-power associated with the Syn bump tell us at which frequency ($\nu_{\text{peak}}^{\text{Syn}}$) most of the AGN electromagnetic power is being released, the parameter $\log(\nu_{\text{peak}}^{\text{Syn}})$ has been extensively used to classify blazars. Following Padovani & Giommi (1995); Abdo et al. (2010), objects

with $\log(\nu_{peak}^{Syn}) < 14.5$, in between 14.5 to 15.0, and > 15.0 [Hz] are called low, intermediate, and high Syn peak blazars, i.e., LSP, ISP, HSP, respectively.

Blazars are by far the largest population of high galactic latitude sources in all Fermi-LAT catalogs and all types of blazars (LSP, ISP, and HSP) have been detected in γ -rays. Nevertheless a relatively large percentage of LSPs still lack detection by Fermi-LAT. The fact that some of these LSPs are relatively bright in radio and show hints of distinct optical polarization properties (Angelakis et al. 2016) has motivated arguments about the existence of a specific class to represent the so-called γ -ray quiet blazars; the latter have a relatively lower polarization fraction. Therefore, current evidence gives us a hint of the jet condition regarding γ -ray undetected blazars, showing they might be connected to relatively less magnetized jets. In particular, Blinov et al. (2015) probed optical polarization swings in connection to periods of enhanced activity in γ -rays, therefore in connection with magnetic field strength and ordering within the jet structure. But the observations of orphan γ -ray flares, which have no counterparts at the low-energy site (optical to X-ray), are a standing challenge for current SSC and EC models when trying to describe blazar variability (Potter 2018). Alternative models such as the Ring of Fire (MacDonald et al. 2017) discuss evidence for a sheath of plasma surrounding the spine of the jet, producing a dominant IR photon field that would undergo IC scattering. Despite that, other works recognize γ -ray undetected blazars as MeV peaked (Paliya et al. 2017), which could be out of reach for Fermi-LAT.

As known, all Fermi-LAT official catalogs are blind with respect to other wavebands, meaning that information about sources detected in other energy bands are not taken into account. Each new γ -ray detection must meet the conservative requirement of being observed at least as a 5σ excess compared to the expected background. This is usually incorporated in the so-called test statistic (TS) parameter (more on sec. 3) translating to a $TS > 25$ requirement for acceptance of new γ -ray sources. This was necessary to avoid spurious detections and misleading associations, especially pre-Fermi-LAT, when the main population of γ -ray emitters was still to be identified.

The situation now has changed since the astrophysics community already recognize blazars as the main population of extragalactic γ -ray emitters. Searches for γ -ray emission in samples of previously known blazars can relax the $TS > 25$ requirement, as discussed in Arsioli & Chang (2017). These authors tested the existence of γ -ray signatures by including more information compared to a pure blind approach and they indeed detected 150 new γ -ray sources. The detection of new sources, together with resolving cases of source confusion, should not be neglected given its direct impact on statistical γ -ray properties of specific populations, particularly for small samples.

Especially in case of LSP blazars, the percentage of γ -ray undetected sources is higher. On average, those blazars have steep γ -ray photon spectral index (Ackermann et al. 2015b) that can compromise the detection of high redshift sources since the γ -ray SED shifts to lower frequencies in the observer rest frame. Also, the absorption of very high energy (VHE) γ -ray owing to the interaction with the extragalactic background light (EBL; Franceschini, A. et al. 2008) may hinder observations with Fermi-LAT. In addition to those possible complications, intrinsic jet proper-

ties (such as the Doppler and beaming factor δ) and the dominant IC regime (either SSC or EC) may also have a large influence on the Fermi-LAT detectability of radio-loud blazars. In fact, Lister et al. (2009) showed that the γ -ray sources detected during the first three months of Fermi-LAT operations are associated with the largest apparent jet speeds (therefore the largest bulk Lorentz factors) as deduced from radio measurements with the Very Large Baseline Array (VLBA). Also, Lister et al. (2015) showed that the γ -ray detection of LSP blazars is relatively less likely when the Lorentz factor is low and the Syn peak is below $10^{13.4}$ Hz. In fact, Sec. 4.5 presents three examples of radio-loud blazars with relatively bright ν_{f_s} Syn peaks that are detectable only during short flare episodes. Those cases could provide hints of the mechanisms behind γ -ray flares and are interesting targets for upcoming missions such as the MeV dedicated e-Astrogram (Tatischeff et al. 2016; De Angelis et al. 2017).

Motivated by the possibility of unveiling new γ -ray sources, we use a complete sample of radio-loud blazars, and consider all cases not yet detected at GeV band for a likelihood analysis with the Fermi Science Tools. Our approach shows that most of the previously γ -ray undetected sources are actually detectable when integrating over 7.5 years of observations or during short periods of their flaring states. We present γ -ray light curves adopting a one month time bin, showing that currently undetected blazars may introduce a dynamic high-energy component to the sky with numerous short periods of γ -ray activity. This might build a considerable portion of the extragalactic γ -ray background (EGB; Ackermann et al. 2015a, 2013) whose origin is still being debated (Fornasa & Sánchez-Conde 2015; Di Mauro & Donato 2015; Di Mauro et al. 2014; Ackermann et al. 2016a). In addition, undetected blazars may add anisotropic contributions to the EGB content especially at small angular scales (Ackermann et al. 2012; Cuoco et al. 2012; Inoue 2014) thus potentially affecting the search for dark matter annihilation or decay signatures in connection to diffuse γ -ray emission from extragalactic large-scale structures (Ando et al. 2014; Prokhorov & Churazov 2014). Indeed, our new detections may complement current understanding of the EGB origin especially for the MeV band where LSP and ISP blazars are more relevant.

Our detailed search for new γ -ray sources also provides a better description of the IC component for many blazars that so far had limited or no γ -ray data available, thus resulting in a measurement of Syn and IC peak-power parameters for nearly all sources (except for five nondetections). Since this radio sample includes the brightest and well-characterized LSP blazars, we study population properties such as the distribution of Syn and IC peak frequencies and peak power, and the distribution of $\log(\nu_{IC}/\nu_{Syn})$ and $\log(\text{Compton dominance})$.

2. Sample description

We consider the complete sample of radio-loud AGN that was studied in detail by Planck Collaboration et al. (2011), consisting of 104 northern and equatorial sources with declination larger than -10° and flux density at 37 GHz exceeding 1 Jy as measured with the Metsähovi radio telescope. We refer to those sources as the Radio-Planck sample and list these sources in table 5 showing their blazar names

Table 1. List of new γ -ray detections and associations for the Radio-Planck sources, following a case by case description in Sec. 4. Columns Source and Redshift list the blazar name and distance as from Massaro et al. (2015). We note that Table 5 brings an extra name reference as from NVSS Radio Catalog (Condon et al. 1998) given that each blazar has a well-defined radio counterpart. Columns $\log(\nu_{peak}^{Syn})$ and $\log(\nu_{peak}^{IC})$ refer to the peak frequency from Syn and IC components measured in Hz. Columns $\log(\nu f_{\nu}^{Syn})$ and $\log(\nu f_{\nu}^{IC})$ correspond to the Syn and IC peak-power measured in erg/cm²/s. Column N_0 list the pre-factor as of eq. 1 in units of ph/cm²/s/MeV when assuming $E_0 = 1000$ MeV. Column Γ list the photon spectral index as of eq. 1. Column TS list the test statistic values associated with the γ -ray signature for each source when integrating over 7.5 years of Fermi-LAT PASS8 observations. All model parameters were derived using the Fermi Science Tools assuming a power-law spectrum within the 0.3-500 GeV energy band. New detections at TS > 20 level are denoted with an “a” flag; new association from better positioning of 3FGL sources are given a “b” flag, faint detections with TS between 10-20 are given a “c” flag; sources only detectable during short flare episodes are given a “d” flag (for those cases, TS values refer to the bright state integrated over one month); and sources that could be confused with a second γ -ray emitter are given an “e” flag.

Source	Redshift	$\log(\nu_{peak}^{Syn})$	$\log(\nu f_{\nu}^{Syn})$	$\log(\nu_{peak}^{IC})$	$\log(\nu f_{\nu}^{IC})$	N_0 (10^{-13})	Γ	TS ^{Pass 8} _{7.5 yrs}
5BZQJ 0359+5057 ^a	1.512	12.1	-10.7	21.3	-10.4	36.6±1.5	2.72±0.04	786.0
5BZQJ 1955+5131 ^a	1.210	12.6	-11.7	20.8	-11.1	7.0±0.7	2.56±0.10	119.7
5BZUJ 0909+4253 ^a	0.670	12.9	-11.5	20.9	-11.7	3.5±0.5	2.62±0.15	74.4
5BZQJ 1153+8058 ^a	1.250	12.6	-12.0	21.1	-11.9	2.1±0.4	2.53±0.19	33.7
5BZQJ 0646+4451 ^a	3.396	11.6	-11.8	20.8 [?]	-11.7	3.8±0.7	3.39±0.24	85.6
5BZQJ 0125-0005 ^a	1.077	12.8	-11.6	20.3	-11.6	2.2±0.5	2.90±0.31	22.5
5BZQJ 0555+3948 ^b	2.365	12.0	-11.8	20.8	-10.9	10.2±1.0	3.12±0.11	195.5
5BZUJ 0433+0521 ^b	0.033	13.8	-10.2	19.8	-10.2	14.4±1.0	2.97±0.08	370.4
5BZQJ 0228+6721 ^b	0.523	12.8	-11.2	21.1	-11.4	8.0±1.0	2.65±0.12	79.4
5BZQJ 2218-0335 ^c	0.901	12.3	-11.3	21.0 [?]	-11.7	2.7±0.6	2.80±0.27	19.9
5BZBJ 0006-0623 ^c	0.347	13.0	-11.1	20.3	-11.9	1.4±0.4	2.13±0.20	17.5
5BZQJ 1038+0512 ^c	0.450	12.0	-11.8	20.8 [?]	-12.1	1.6±0.6	2.79±0.38	10.1
5BZQJ 0010+1058 ^d	0.089	14.5	-10.7	20.5	-10.8	4.1±1.9	3.22±0.53	26.0*
5BZUJ 0241-0815 ^d	0.005	13.9 [?]	-10.3	20.9 [?]	-10.6	6.3±0.2	1.64±0.01	12.0*
5BZQJ 2136+0041 ^d	1.941	10.8	-11.7	21.2	-11.2	19.9±2.0	2.46±0.10	7.5*
5BZQJ 1642+6856 ^e	0.751	12.5	-11.6	20.1 [?]	-12.3	9.1±4.0	2.31±0.28	8.3

from 5BZcat (Massaro et al. 2015), and their NVSS¹ radio counterpart. Out of these sources, 83 have a confirmed γ -ray counterpart in at least one of the Fermi-LAT (Atwood et al. 2009) catalogs, i.e., 1FGL, 2FGL, and 3FGL (Abdo et al. 2010; Ackermann et al. 2011; Acero et al. 2015) or 2FHL and 3FHL (Ackermann et al. 2016b; Ajello et al. 2017). However, the nondetection by Fermi-LAT of the remaining 21 equally bright radio-loud AGN with similar radio-to-optical SED is intriguing, rising discussions on both the nature of the high-energy emission in blazars and the efficiency of Fermi-LAT in solving faint γ -ray sources (Lister et al. 2015). It has been argued that LSP blazars with $\nu_{peak} < 10^{13.4}$ Hz may show a typical IC peak below 0.1 GeV out of the Fermi-LAT sensitivity bandwidth (0.1-500 GeV), so that we can only probe the very end of the IC component (Paliya et al. 2017).

3. γ -ray analysis of undetected sources

In a blind analysis, the spectral parameters of a hypothetical source, such as normalization and photon spectral index, and also the source position itself (R.A. and Dec.) are all free parameters that have to be optimized during the data analysis. We might be able to reduce the uncertainty, however, with respect to position since we know multiple γ -ray blazar candidates that have already been identified from multifrequency observations from radio up to X-rays. Actually, a total of 21 sources in our Radio-Planck sample

do not have a γ -ray counterpart in previous Fermi FGL catalogs. Those constitute a set of 21 seed fixed positions, for which we test the existence of relevant γ -ray signatures. This method has been successfully tested for a set of 400 γ -ray candidates (Arsioli & Chang 2017) preselected from a sample of HSP blazars, resulting in 150 new detections.

We performed a likelihood analysis integrating over 7.5 years of Fermi-LAT observations in the 0.3-500 GeV band using Pass 8 data release (Atwood et al. 2013), and assuming the γ -ray spectrum of a new source could be described by a power-law model as

$$\frac{dN}{dE} = N_0 \left(\frac{E}{E_0} \right)^{-\Gamma}, \quad (1)$$

where E_0 is a scale parameter (also known as pivot energy), N_0 is the pre-factor (normalization) corresponding to the flux density in units of ph/cm²/s/MeV at the pivot energy E_0 , and Γ is the photon spectral index for the energy range considered. Both Γ and N_0 are set as free parameters and further adjusted by the fitting routine *gtlike*. Source positions and $E_0 = 1000$ MeV are set as fixed parameters, therefore constants for the likelihood analysis. In the source-input xml file, all sources within 10° from the candidate had both Γ and N_0 parameters flagged as free². Therefore the 3FGL models of these sources, which are based on four years of observations were adjusted, since

² In this regard we are following recommendations from Fermi Science Tools user guide https://fermi.gsfc.nasa.gov/ssc/data/analysis/scitools/binning_likelihood_tutorial.html, which recommends setting free parameters at least within 7° from the source of interest. This is a consequence of the

¹ National Radio Astronomy Observatory Very Large Array Sky Survey, the so-called NVSS Catalog

we integrated over 7.5 years of data. This particular choice increases the computational burden of the analysis, but it is crucial for adapting the model maps to the extra 3.5 years of exposure that is being considered. Results are shown in Table 1, listing only the 16 cases that had no known counterpart from previous γ -ray catalogs and which we now describe case by case in this work. Also we note that Table 5 holds the description for the entire Radio-Planck sample.

Since we are dealing with sources that are predominantly LSP blazars, we should expect them to have steep γ -ray SED (in $\log(\nu f_\nu)$ versus $\log(\nu)$ plane) as observed from the correlation in Γ versus $\log(\nu_{\text{peak}}^{\text{Syn}})$ plane (Acero et al. 2015), where LSP sources dominate the $\Gamma > 2.0$ side. The parameter N_0 represents the flux at 1 GeV (given our choice for E_0). Therefore new detections are expected to be on the border or below Fermi-LAT four year sensitivity limit³, which is $E^2 dN/dE \approx 2.0 \times 10^{-12}$ erg/cm²/s at 1 GeV, i.e., $dN/dE \approx 12.5 \times 10^{-13}$ ph/cm²/s/MeV. Following our results as reported in Table 1, few cases have N_0 above the Fermi-LAT four year sensitivity level. In particular 5BZQJ 0359+5057 and 5BZUJ 0241-0815 have larger N_0 , which is clearly a consequence of an enhanced γ -ray activity reported just after 2013 (out of the integration period used to build the 3FGL catalog) as discussed in Sec. 4.1 and 4.5. Another three sources flagged with “b” have N_0 close to the 3FGL sensitivity border; those are actually detected in the 3FGL catalog but with large position uncertainty, which lead them to be unassociated in previous catalogs.

Positive γ -ray signatures were first evaluated based on test statistics (TS) values as defined by Mattox et al. (1996): $TS = -2\ln\left(\frac{L_{(\text{no source})}}{L_{(\text{source})}}\right)$, where $L_{(\text{no source})}$ is the likelihood of observing a certain photon count for a model without the candidate source (the null hypothesis), and $L_{(\text{source})}$ is the likelihood value for a model with the additional candidate source at the given location. The reported TS values correspond to a full band fitting, which constrains the whole spectral distribution along 0.3-500 GeV to vary smoothly with energy and assuming no spectral break. Considering that we have a good description of the Galactic and of the extragalactic diffuse components, this is a measure of how clearly a source emerges from the background, also assessing the goodness of free parameters fit.

A $TS \approx 25$ is equivalent to a $4\text{--}5\sigma$ detection, depending on the strength of the background in the region (Abdo et al. 2010), and only cases with $TS > 25$ are considered by the Fermi-LAT team as a positive detection of a point-like source. Following the discussion on Arsioli & Chang (2017), we analyzed γ -ray signatures down to $TS=10$, which are spatially consistent with blazars already known from other energy bands and double checked these with TS maps.

A TS map consists of a pixel grid where the existence of a point-like source is tested for each pixel, and each grid bin is evaluated using a likelihood analysis⁴. Since the PSF

large point spread function (PSF), especially at low-energy threshold, which can overlap with nearby sources. Therefore, in order to get a confident description of a particular source, we properly fit and adjust the whole environment around it.

³ 3FGL sensitivity considering the instrument response function (P7REP-SOURCE-V15), as described at Fermi-LAT repository http://www.slac.stanford.edu/exp/glast/groups/canda/archive/p7rep_v15/lat_Performance.htm

⁴ For a complete description of the Fermi Science Tools, check: <https://fermi.gsfc.nasa.gov/ssc/data/analysis>.

improves with energy, we worked with $E > 500$ MeV photons to help us determine the TS peak position with better precision than working at lower Fermi-LAT bandwidth (down to 100 MeV). Thus the map alone tests the existence of a point-like source emerging from a flat low-TS background.

We enhanced the γ -ray characterization of the Radio-Planck sample by $\approx 15\%$, since we now describe ten new detections of steady sources as discussed in Sec. 4.1, Sec. 4.2, and Sec. 4.4; three new associations from improved position of previously known 3FGL sources as discussed in Sec. 4.3; and three detections of sources with isolated flaring activity as discussed in Sec. 4.5. In the following discussion we present fitting parameters, SEDs, light curves for most relevant cases, and TS maps for all sources. We comment on four cases where we find poor evidence of γ -ray signature, which is probably related to high redshift, IC peak at MeV band, and low galactic latitude hindering the detection.

For the light curves, we usually considered a time bin of approximately 30 days, and estimated the corresponding flux and errors only when the TS per bin was larger than 4.0. When this condition was not satisfied, an upper limit to the flux was calculated using the integral method (provided by the Fermi Science Tool), which takes into account the background level and spectral properties of the test source.

4. New γ -ray detections, validation, and association

We present new γ -ray signals down to $TS \approx 10$ level. We also describe one case of source confusion, solve three cases of unassociated 3FGL sources, and comment on the non-detections as well. Table 1 shows the power-law parameters resulting from the fit in the 0.3-500 GeV energy band, together with redshift of the counterpart, Syn, and IC peak frequency (ν_{peak}), and flux density (νf_ν) for all cases studied. For each source, we present a TS map together with the γ -ray SED with a polynomial fit for both Syn and IC component. Following Giommi et al. (2012b), when fitting the nonthermal component we also account for optical and UV thermal emission due to accretion using the composite optical spectrum built by Vanden Berk et al. (2001). This thermal template is based on 2200 optical spectra of radio-quiet quasars (QSOs) taken from the SDSS database and its expected soft X-ray emission, from Grupe et al. (2010).

The TS maps are calculated considering only photons with $E > 500$ MeV, which is a good choice to evaluate the TS spatial distribution for these radio sources, since they usually have a photon spectral index in the range $2.0 < \Gamma < 3.0$. Whenever possible, we also use $E > 1.0$ GeV photons (or higher) to improve the localization of γ -ray signatures. We call attention to the fact that for most cases we are dealing with relatively faint γ -ray sources, therefore the TS distribution could peak at a position slightly offset from its counterpart. An offset is expected given the uncertainty introduced by the large PSF, which is on the order of 1.4° at 500 GeV (Atwood et al. 2013) and 0.81° at 1 GeV level. Following the discussion in Abdo et al. (2010) what is important to ensure a proper match is that the 68% confinement region for the γ -ray signature should enclose the counterpart blazar. This is explicitly shown case by case to help validate our new detections and associations.

We show the light curves with monthly bins for those cases for which we identify a γ -ray flaring activity during

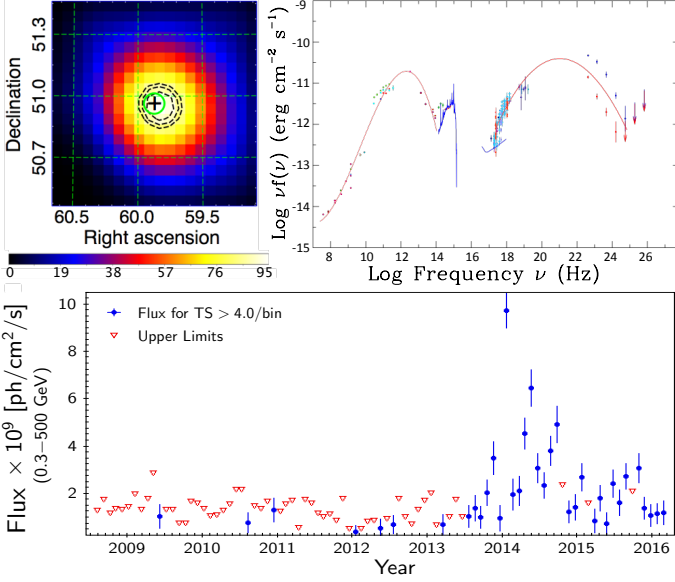


Fig. 1. 5BZQJ 0359+5057. Top left: TS map considering only $E > 0.5$ GeV photons with black dashed lines representing 68%, 95%, and 99% containment regions for the γ -ray signature (used for all further TS maps), considering the brightest period from 2014 to 2015; 5BZQJ 0359+5057 is marked with a circle centered at “+”. Top right: The SED with a polynomial fit to the mean Syn and IC components; the blue-bump feature between 10^{14} and 10^{18} Hz (Vanden Berk et al. 2001) for a source at $z=1.512$. In the γ -ray band, red points represent the SED before flaring (before 2013), while blue is for the flaring period (after 2013). Bottom: 0.3-500 GeV light curve along 7.5 yrs of observations with bins of 30 days; red points represent upper limit flux.

the 7.5 yrs covered by Fermi-LAT. Light curves are computed with likelihood analysis, therefore the background is extracted and flux points are calculated only for time bins that have $TS > 4$. For all cases we compute upper limits and errors bars using the integral method assuming a 95% confidence level, as provided by the Fermi Science Tools. When relevant for the discussion, we also show the significance of the γ -ray signatures based on the 3FGL setup (i.e., likelihood analysis with 4.0 yrs of Pass 7 data) to test if those sources could have been identified previously.

4.1. Notes on individual objects

We present a detailed description for the new γ -ray detection, which showed $TS > 20$ when integrating over 7.5 years of observations. Those cases are relatively isolated, meaning there are no other close by γ -ray counterparts that could contaminate the observed signatures. For the discussion we include TS maps, light curves, and spectral points. Together, those elements build an entire picture, not only validating and describing their γ -ray properties, but also explaining (whenever necessary) why those sources were not previously detected, showing examples on how the data treatment is refined with multifrequency information, leading to more efficient use of public databases.

5BZQJ 0359+5057. Computing a TS map in the 0.5-12 GeV energy range (Fig. 1), we identified a bright point-like source clearly emerging from a low and flat TS background. The light curve plotted in Fig. 1, shows that the

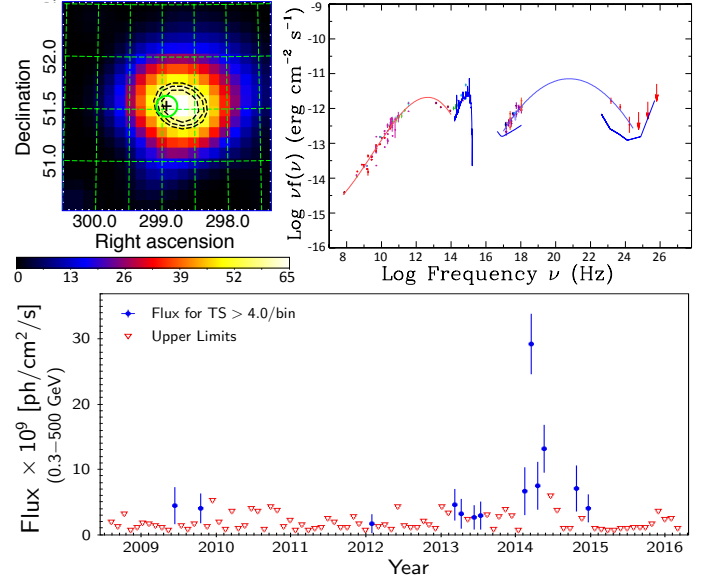


Fig. 2. BZQJ 1955+5131. Top left: TS map considering only $E > 0.5$ GeV photons, during the high-state period between 2014 and 2015. Top right: SED for 5BZQJ 1955+5131 at $z=1.21$, with the new γ -ray spectrum in the 0.3-500 GeV band. As example, in the 10^{22} - 10^{26} Hz band (0.1-500 GeV) we show the Fermi-LAT sensitivity limit when integrating over four year of observations. Bottom: The γ -ray light curve for 5BZQJ 1955+5131 along 7.5 yrs of observations and with time bin of 30 days.

source 5BZQJ 0359+5057 (4C +50.11) was undetectable by Fermi-LAT, most of the time with the exception of the period between June 2013 and April 2016 when it underwent a phase of strong γ -ray activity. This is consistent with its nondetection up to the 3FGL catalog (since 3FGL only integrate observations from Aug. 2008 up to Aug. 2012).

To reproduce the 3FGL setup, we performed a likelihood analysis with Pass 7 data, integrating only during the first four years of observations. As result we found $TS_{4.0 \text{ yrs}}^{Pass 7} = 15.2$, with model parameters $N_0 = 8.1 \pm 2.2 \times 10^{-13}$ ph/cm²/s/MeV and $\Gamma = 2.55 \pm 0.19$, using $E_0 = 1000$ MeV as pivot energy. Hence, this source was out of the 3FGL catalog simply because it did not meet the $TS > 25.0$ criteria. We also noticed that the parameters estimated at the time of 3FGL catalog were already in good agreement with those we present on Table 1, showing that γ -ray signatures at 10 to 25 TS level contain rich information, as discussed in Arsioli & Chang (2017).

As an exercise, we used a setup similar to 3FGL (integrating over 2008-2012) but now with PASS 8 data. This results in a firm detection with $TS > 25$ and the γ -ray SED shown as red points in Fig. 1 (bottom). This give us a solid idea on how the Pass 8 data release brings way relevant enhancements for the description of the γ -ray sky.

5BZQJ 1955+5131. This blazar shows a strong γ -ray signal when integrating over 7.5 yrs with Pass 8 data, but from the light curve (Fig. 2) we measured significant flaring activity only after 2014. A likelihood analysis integrating Pass 7 data from Aug. 2008 up to Aug. 2012 (hereafter we refer to this as the 3FGL setup) have shown $TS_{4.0 \text{ yrs}}^{Pass 7} \approx 5.0$, and therefore this source is out of the 3FGL catalog because of its variability. In addition, this blazar is close to the galactic plane ($b = 11.7^\circ$), where the low-energy dif-

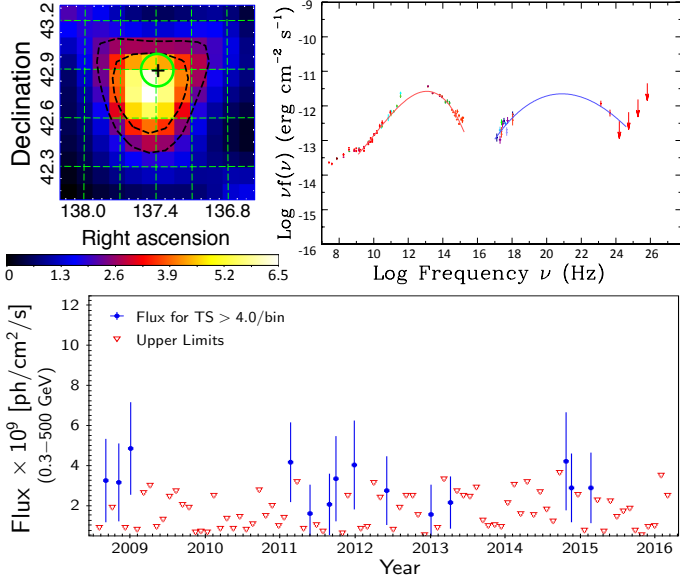


Fig. 3. 5BZUJ 0909+4253. Top left: TS map considering only $E > 0.5$ GeV photons during the brightest period, from January 6 to February 6, 2009. Top right: SED for 5BZUJ 0909+4253, $z=0.670$. Bottom: The γ -ray light curve along 7.5 yrs of observations.

fuse background is more intense thus hindering detections of faint γ -ray sources. In fact, owing to larger background levels, the Fermi-LAT sensitivity in the Galactic plane region is lower than at high Galactic latitude⁵.

5BZUJ 0909+4253. This blazar is strongly detected when integrating over 7.5 yrs with Pass 8 data ($\text{TS}_{7.5 \text{ yrs}}^{\text{Pass 8}} = 74.4$), but shows no strong flaring activity as can be seen in Fig. 3. A likelihood analysis with the 3FGL setup gives $\text{TS}_{4.0 \text{ yrs}}^{\text{Pass 7}} \approx 14.2$, with power-law parameters $N_0 = 2.4 \pm 0.8 \times 10^{-13}$ ph/cm²/s/MeV, $\Gamma = 3.04 \pm 0.38$, using $E_0 = 1000$ MeV as pivot energy, which agrees with values reported in Table 1. This is another example for which it would be beneficial to have preliminary information about faint signatures with TS in between 10 to 25, which were already available with 4 yr Pass 7 data. The TS map (Fig. 3) confirms that the observed γ -ray signature emerges as a point-like source from a low-TS background.

5BZQJ 1153+8058. From the light curve (bottom panel of Fig. 4) this source shows γ -ray activity only in 2014, which is consistent with its noninclusion in the 3FGL catalog (3FGL covers the period of 08/2008–08/2012). A likelihood analysis with 3FGL setup results in null detection. For this case, we are likely probing the peak of a transient γ -ray activity during the year 2014, and smoothing out the signal along 7.5 years of binned analysis. The detection of a steady high-energy component (non-flaring state) is currently limited by the Fermi-LAT sensitivity. Therefore, the parameters reported on Table 1 embody the mean γ -ray spectrum behavior and represent a good example of how γ -ray activity is washed out for the building of current high-energy catalogs that integrate Fermi-LAT observations over 4.0 year (in case of the 3FGL) to 7.5 years. We built a TS map (top left in Fig. 4) integrating along

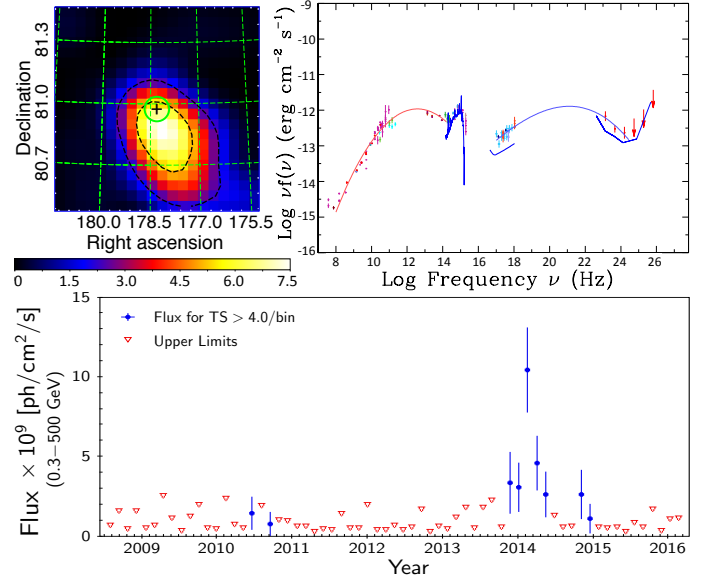


Fig. 4. 5BZQJ 1153+8058. Top left: TS map using $E > 3.0$ GeV photons collected during the 2014 flaring period. Top right: SED for 5BZQJ 1153+8058 also showing the template for thermal emission from accretion in the range $10^{14} - 10^{18}$ Hz assuming $z=1.250$. Bottom: The γ -ray light curve for 5BZQJ 1153+8058 along 7.5 yrs.

the whole year of 2014, showing that the blazar position is compatible with the γ -ray signature within the 68% containment region. This case in particular allowed us to use $E > 3.0$ GeV photons instead of $E > 500$ MeV, providing improved localization.

5BZQJ 0646+4451. Although this source is located in a relatively crowded region close to the Galactic plane ($|b|=17.9^\circ$), the low-energy detection is very significant with $\text{TS}_{7.5 \text{ yrs}}^{\text{Pass 8}} \approx 80$ in the 300–550 MeV energy bin alone. We found no significant flaring activity during the 7.5 yrs of observations with Fermi-LAT, and the period with the most significant γ -ray signature extends from October 25 to November 30, 2010. The highest energy photons detected from this region are ~ 10 GeV, and therefore we built a TS map in the 500 MeV - 12 GeV energy range (Fig. 5, left panel). The γ -ray signature emerges as a point source fully compatible with the blazar position. In particular, the γ -ray counterpart has high redshift of $z=3.396$, and absorption due to EBL might hinder the detection of VHE photons.

A likelihood analysis using the 3FGL setup has shown $\text{TS}_{4 \text{ yrs}}^{\text{Pass 7}} = 20.3$, with pivot energy $E_0 = 1000$ MeV, pre-factor $N_0 = 2.6 \times 10^{-13}$ ph/cm²/s/MeV, and $\Gamma = 3.61$, which is in good agreement with the parameters presented in Table 1. This is another example of low-significance γ -ray signature with TS between 10 and 25, which would have been beneficial to report on without compromising the spectral description (that can be refined with longer integration time as shown).

5BZQJ 0125-0005. This source has been detected with $\text{TS} \approx 20$ when integrating over 7.5 yrs with Pass 8 data. Its light curve does not present strong flaring episodes, but we identify the most relevant bin as July 31 to August 31, 2013, as used to build the TS map. Although the TS value is below 25, we consider it a firm detection since the TS map (6) clearly shows the γ -ray point-like signature emerge from a low-TS background, and the 68% confinement region is

⁵ For a description on the Fermi-LAT performance check https://www.slac.stanford.edu/exp/glast/groups/canda/lat_Performance.htm

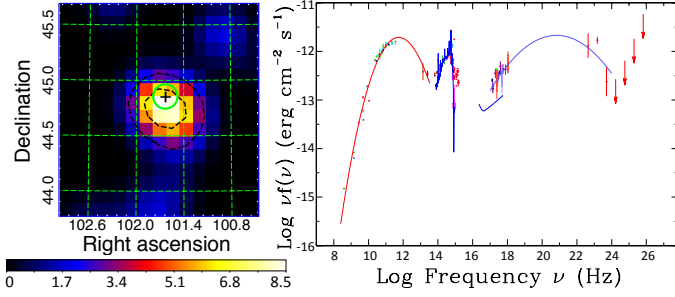


Fig. 5. 5BZQJ 0646+4451. Left: TS map considering 500 MeV to 12 GeV photons and integrating over the flaring period from October 25 to November 30, 2010. Black dashed lines represent 68% and 95% confinement regions for the γ -ray signature. Right: SED for 5BZQJ 0646+4451, also showing the blue bump template assuming $z=3.396$.

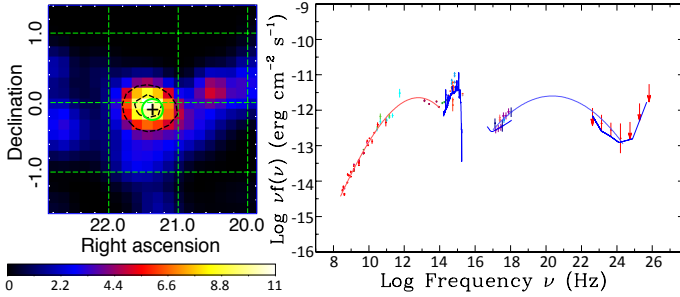


Fig. 6. 5BZQJ 0125-0005. Left: TS map considering only $E > 500$ MeV photons and integrating data along the brightest month from July 31 to August 31, 2013. Black dashed lines show the 68% and 95% confinement region for the γ -ray signatures. Right: Multifrequency SED for 5BZQJ 1153+8058 with the blue bump template corresponding to $z=1.077$

compatible with the blazar position. A likelihood analysis with the 3FGL setup gives $TS_{4\text{ yrs}}^{Pass 7} = 12.9$ with parameters $E_0 = 1000$ MeV, $N_0 = 2.8 \times 10^{-13}$ ph/cm²/s/MeV, and $\Gamma = 2.68$, again in agreement with parameters from Table 1.

4.2. Source confusion

We discuss a case in which source confusion involving a steep and a hard spectrum γ -ray source is likely present. Even though no γ -ray source is reported within 1° of 5BZQJ 1642+6856 in any of the FGL catalogs, our likelihood analysis finds a γ -ray signature matching the position of this source, which is located only ~ 10 arcmin from the HSP blazar 2WHSPJ 164014.8+685233. Indeed, the high-energy $E > 1.0$ GeV TS map (Fig. 7 in top left panel) reveals a dominant γ -ray signature coincident with the 2WHSP source, however extending toward the position of 5BZQJ 1642+6856. We then consider photons in the 0.1-500 GeV band and a likelihood function including two nearby point-like emitters, which gives us an estimate of the γ -ray spectral properties for each source as shown in Table 2. Despite the low statistical significance associated with BZQJ 1642+6856 γ -ray signature ($TS < 10$), we note that the photon spectral index Γ estimated for the pair 5BZQ & 2WHSP is consistent with the hypothesis of confusion between a steep and a hard component as expected for nearby LSP and HSP blazars.

As a consistency test, we built an additional high-energy TS map ($E > 1$ GeV) by adding a point-like source at the 2WHSP position modeled as a power-law with the same parameters as from Table 2, such that the 2WHSP γ -ray signature is now part of the background model. As a result (Fig. 7, top right panel) we reveal a residual point-like signature consistent with 5BZQJ 1642+6856 within the 68% confinement radius. All together, it suggests this might be a case of source confusion, which is hard to resolve with currently available data. Since those γ -ray signatures have not been reported in previous high-energy catalogs, we present 2WHSPJ 164014.8+685233 as a new detection and 5BZQJ 1642+6856 as a relevant signature, whose resolved SEDs are shown in Fig. 7 (middle and bottom panels).

Table 2. Source model parameters derived from the Fermi Science Tools assuming a power-law to describe the γ -ray spectrum within the 0.1-500 GeV energy band, with N_0 given in ph/cm²/s/MeV, and assuming $E_0 = 1000$ MeV.

Source	N_0 (10^{-14})	Γ	TS
2WHSPJ 164014.8+685233	7.4 ± 0.4	1.73 ± 0.18	35.7
5BZQJ 1642+6856	9.1 ± 4.0	2.31 ± 0.28	8.3

4.3. New associations from improved positions determination

Arsioli & Chang (2017) showed that high-energy TS maps can be used to improve the localization for many γ -ray signatures currently listed in FGL catalogs. It is well known that the Fermi-LAT detector (Atwood et al. 2009) is characterized by a highly energy-dependent point spread function (PSF), which contains 68% of the 1 GeV events within 0.8° , decreasing afterward with a trend $\propto E^{-0.8}$ up to 10's GeV, and finally roughly constant at 0.1° up to the highest energies considered in this paper. Therefore, working with $E > 1$ GeV allows us to better constrain the position associated with the γ -ray signature, which helps solve cases of source confusion. This is particularly important for unassociated 3FGL (Acero et al. 2013) that are actually counterparts of close by blazars. We present two such cases, noting that an approach based on the prior multifrequency identification of nearby blazars certainly improve the γ -ray associations with potential counterparts.

3FGLJ 0432.5+0539. We present an improved position reconstruction for the source 3FGLJ 0432.5+0539, for which no association is reported on the 3FGL catalog. We build a TS map using only photons with $E > 2$ GeV and removing the 3FGL source from the background model.

Fig. 8 shows that the 68% containment region for the γ -ray signature is fully consistent with the position of BZUJ 0433+052, while the 3FGL position (magenta dashed circle on the top left panel) is well outside of the 99% confinement region for the high-energy TS peak. Although part of the improvement could be ascribed to the better instrument response function (IRF) and event selection of the Pass 8 data release with respect to the Pass 7 as used for 3FGL production, it should be noted that high-energy TS maps has proven to provide a significant contribution in source positioning.

3FGLJ 0556.2+3933. This is another case of a 3FGL source with no association that benefits from an improved position reconstruction. As shown in the top right panel of

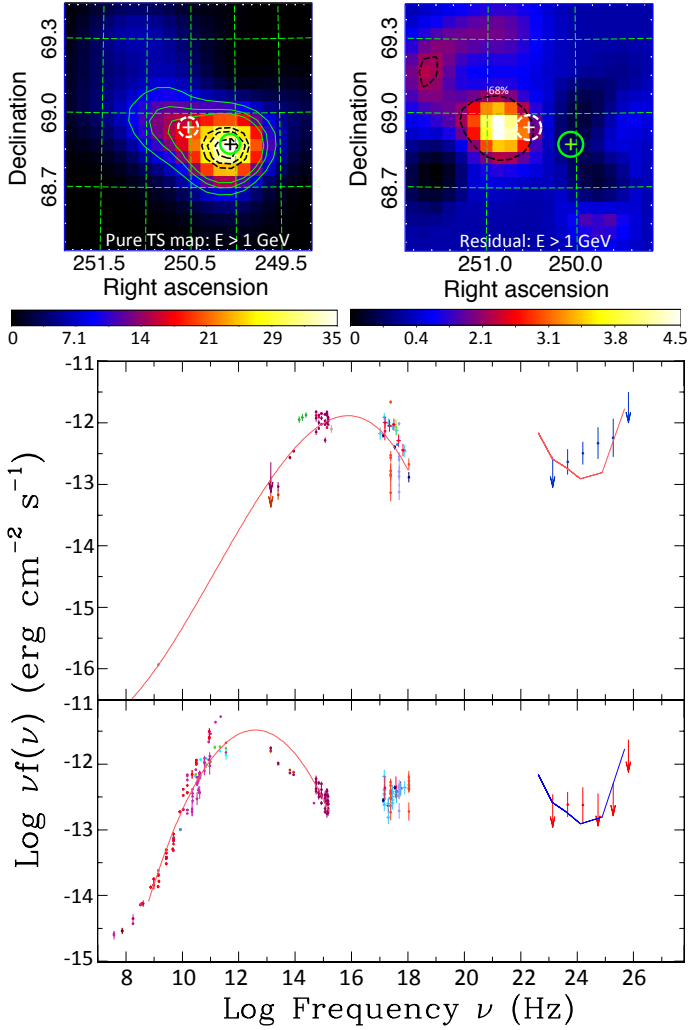


Fig. 7. BZQJ 1642+6856. Top left: TS map for $E > 1.0$ GeV. The green thin lines show contours corresponding to TS values of 15, 12, 8, and black dashed lines represent 68%, 95%, and 99% containment region. Top right: Residual TS map for $E > 1$ GeV considering a source placed at the 2WHSP position, indicated with green cross, as part of the γ -ray background; in this case the black dashed line corresponds to the 68% confinement radius for the γ -ray source, while the white cross indicates the position of BZQJ 1642+6856. Middle and bottom: SEDs for 2WHSPJ 1640+6852 for which no optical identification is available yet, and BZQJ 1642+6856 with $z = 0.751$. The upper limits on the γ -ray spectra have been calculated only for energy bins with low significance.

Fig. 9, there is no relevant radio or X-ray counterpart that is compatible with the 95% positional error ellipse for the 3FGL source (dot-dashed line). However, a powerful blazar is only ~ 18 arcmin away. Indeed, building a TS map using high-energy photons (with $E > 1$ GeV) we are able to show that the 68% confinement radius for the γ -ray signature is fully consistent with the position of 5BZQJ 0555+3948. In addition, the γ -ray spectrum we obtained is compatible with expectations for the end tail of the IC bump.

3FGLJ 0228.5+6703 and its correct counterpart.

Blazar 5BZQJ 0228+6721 had no γ -ray counterpart in previous FGL catalogs, however a γ -ray source at its vicinity

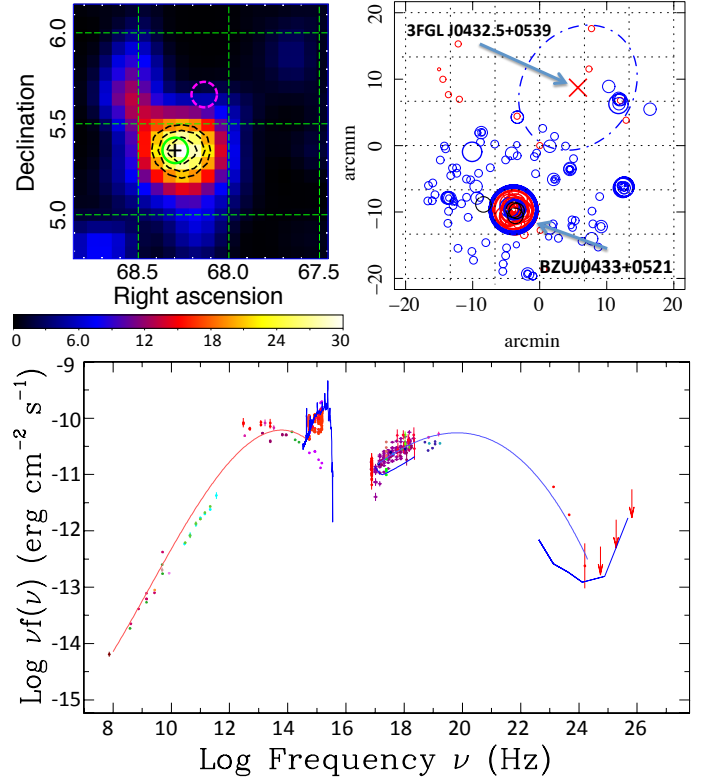


Fig. 8. 5BZUJ 0433+0521. Top left: TS map built using only photons with $E > 2.0$ GeV; Black dashed lines show 68%, 95%, and 99% confinement regions. The position of a nearby BZU source is highlighted by the green circle around the “+” marker, while 3FGL detection is center on the magenta dashed circle. Top right: an image obtained from the SSDC Sky-Explorer showing that 5BZUJ 0433+0521 position is inconsistent with 3FGLJ 0432.5+0539 detection also taking into account its 95% positional uncertainty (dot-dashed ellipse). Blue and red circles represent respectively X-ray and radio frequency detections in the same region as taken from publicly available data. Bottom: SED for 5BZUJ 0433+0521 with blue bump template for $z=0.033$.

was detected (1FGLJ 0233.4+6654) but with no consistent position. In this same region the source 3FGLJ 0228.5+6703 has been associated with a radio source GB6J 0229+6706 (GB: from Green Bank 4.85 GHz northern sky survey, Gregory et al. 1996) which is within the 3FGL error circle (dot-dashed line, Fig. 10 top left). This field is difficult to study because it is very close to the Galactic plane (at latitude $b \sim 6^\circ$) and the intense low-energy diffuse γ -ray background can hinder both the source localization and detection when integrating over the full energy bandwidth.

Since the 3FGL position is only 5.94 arcmin from the blazar, we investigated whether we could improve the γ -ray localization of this source working with $E > 500$ MeV photons, benefiting from lower background intensity, improved PSF, and longer integration time (from 4.0 to 7.5 years). We calculated the $E > 500$ MeV TS map (Fig. 10, top left) showing that the 68% containment region for the γ -ray signature is compatible with 5BZQJ 0228+6721 (while GB6J 0229+6706 is out of the 99% containment region) and therefore the 3FGL association should be revised. We recalculated the γ -ray SED (Fig. 10, bottom) assuming a single

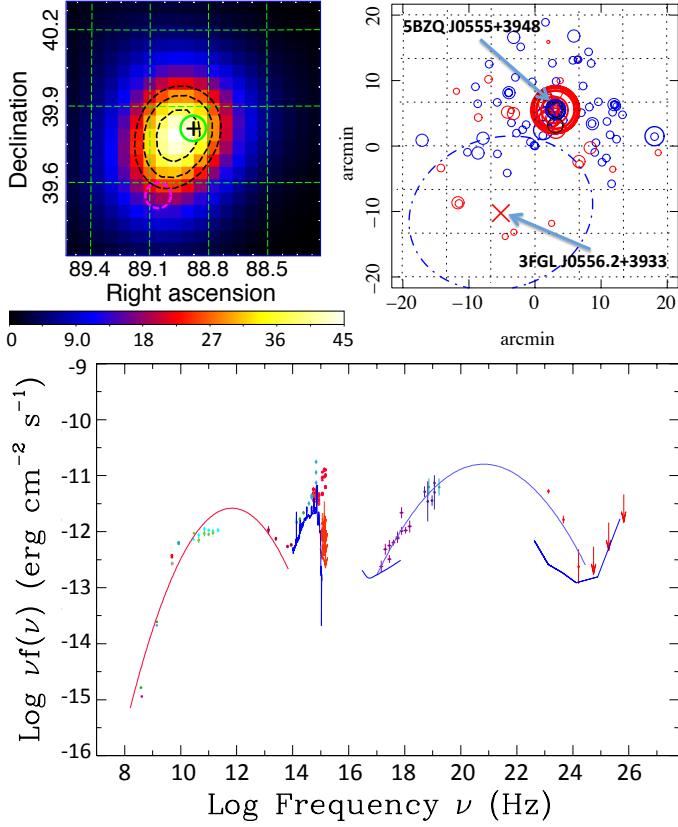


Fig. 9. 5BZQJ 0555+3948. Top right: Sky-Explorer view, showing 3FGLJ 0556.2+3933 indicated as a red cross, while 5BZQJ 0555+3948 is outside the error circle associated with the γ -ray signature from 3FGL database. Blue and red circles represent X-ray and radio detections in this region. Top left: TS map, $E > 1.0$ GeV with improved position for the γ -ray signature; Black dashed lines show the 68%, 95%, and 99% confinement region for the γ -ray signatures. The dashed magenta circle corresponds to the 3FGLJ 0556.2+3933 position, while the green circle is centered on the position of 5BZQJ 0555+3948 marked as black cross. Bottom: SED for 5BZQJ 0555+3948, where the blue bump template assumes $z=2.365$.

source with position corresponding to 5BZQJ 0228+6721, and found it is consistent with the end-tail IC bump.

4.4. Low-significance γ -ray excesses

We present sources showing faint γ -ray signature $10 < TS < 20$ when integrating over 7.5 years of Fermi-LAT observations. It is important to report on faint detections, especially to clarify if these sources are actually γ -ray active, but under the TS limit currently used by the Fermi team, or if they are really quiet in the γ -ray band. Also, low-significance γ -ray detections help to complement the source number count in the faint end of the $\log N$ - $\log S_\gamma$, and therefore can impact estimates of the contribution of blazars to the $E < 1$ GeV extragalactic γ -ray background. We found the light curves for 5BZQJ 2218–0335, 5BZBJ 0006–0623, and 5BZQJ 1038+0512 show short-lived activity at the timescale of a month, and we report on their TS maps and preliminary power-law modeling.

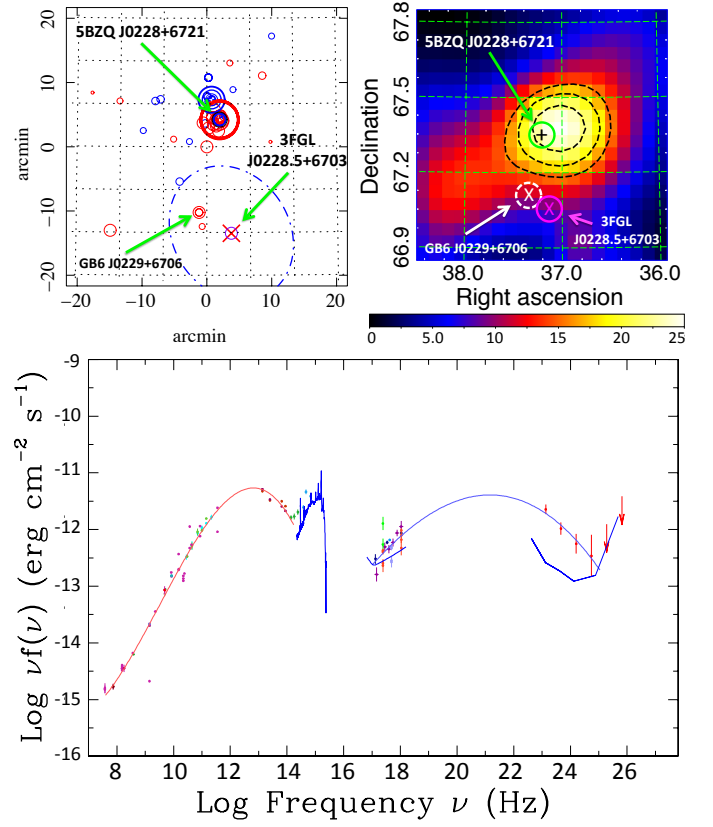


Fig. 10. 5BZQJ 0228+6721. Top left: Sky Explorer view, showing 3FGLJ 0228.5+6703 marked with “x” symbol, and dashed line for the error circle associated with the 3FGL γ -ray signature. We also highlight the positions of GB6 J0229+6706 and 5BZQJ 0228+6721. The red and blue circles represent radio and X-ray detections in the field. Top right: TS map considering $E > 500$ MeV photons, with dashed lines representing 68%, 95%, and 99% containment region for the γ -ray signature; 5BZQJ 0228+6721 is center at “+” matching the TS peak position. Bottom: SED for 5BZQJ 0228+6721, with blue bump assuming $z=0.523$.

Table 3. Source model parameters from Fermi Science Tools, assuming a power-law to describe the γ -ray spectrum within 0.1–500 GeV, with N_0 given in [ph/cm²/s/MeV], and using $E_0 = 1000$ MeV as pivot energy. Case marked with * is probably an spurious detection.

Source	z	N_0 (10^{-13})	Γ	TS
5BZQJ 2218–0335	0.901	2.7 ± 0.6	2.80 ± 0.27	19.9
5BZBJ 0006–0623	0.347	1.4 ± 0.4	2.13 ± 0.20	17.5
5BZQJ 1927+7358*	0.302	1.8 ± 0.5	2.61 ± 0.26	16.4
5BZQJ 1038+0512	0.45	1.6 ± 0.6	2.79 ± 0.38	10.1

As seen from the TS maps, only 5BZQJ 1927+7358 is out of the 68% containment for the γ -ray signature. In this case, the observed TS value (table 3) when integrating over 7.5 yrs of observations can be attributed to residual signal from an unidentified close-by γ -ray source. For now, we consider it as a likely spurious signal.

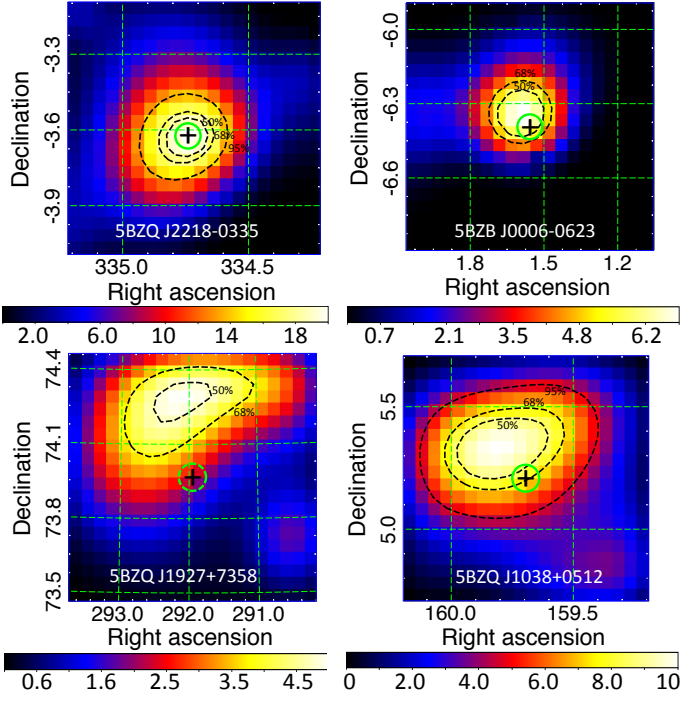


Fig. 11. TS maps for the low-significance γ -ray detections using only $E > 500$ MeV photons. For each case the blazar position is highlighted with thick green circle center at “+”. Black dashed lines show the 50%, 68%, and 95% containment radius for the γ -ray signature.

4.5. Detections during flaring episodes

We present the γ -ray analysis for three radio-loud blazars that have relatively bright νf_ν Syn peak, 5BZQJ 0010+1058, 5BZUJ 0241-0815, and 5BZQJ 2136+0041, for which the detection with Fermi-LAT was expected but not yet reported. This brings us to an important consideration about the role of short-lived flares at monthly timescales since a considerable portion of γ -ray active sources could be still undetected simply because their short-lived signatures are diluted below the sensitivity threshold when integrating Fermi-LAT observations over long exposure time.

5BZQJ 0010+1058 This object is a radio-loud source (also known as MRK 1501) for which γ -ray detection was expected since it is a relatively bright and close-by blazar with $\nu f_\nu = 10^{-10.7}$ erg/cm²/s and $z=0.089$. When integrating over 7.5 years, no γ -ray signature was evident ($TS \approx 0.0$). Nevertheless its light curve (Fig. 12, bottom) shows fast (within the timescale of a month) and relatively bright flares, almost reaching two orders of magnitude variability with respect to the background. When running a likelihood analysis integrating only for the duration of the flare, June 18 2009 to October 31 2010, we could characterize the short-lived γ -ray spectrum, reaching $TS \approx 26$ for the single month bin of June 2010. In this case (Fig. 12, top right), the upper limits calculated for the γ -ray SED are less restrictive, since we are integrating over a single month. We checked for coincident X-ray measurements from *Swift* (along the γ -ray flaring activity from June 2009 to May 2010), but for the observations made in February 2010 we could find no sign of strong X-ray flaring. This is a good example of transient γ -ray source, which we could only de-

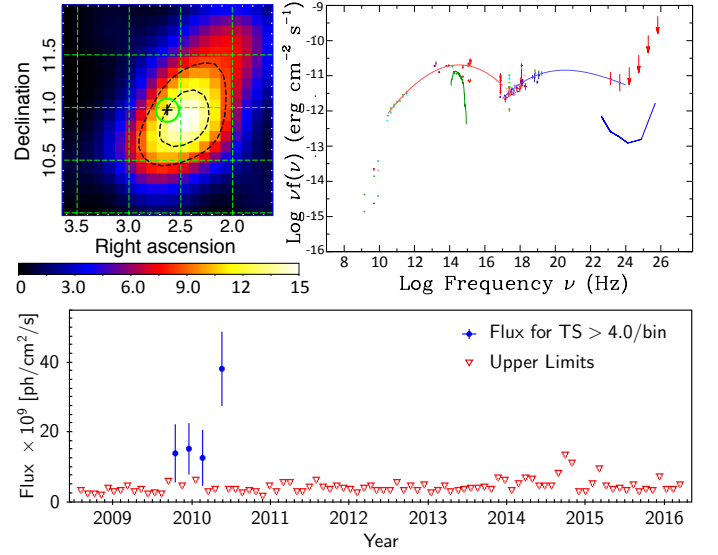


Fig. 12. 5BZQJ0010+1058. Top left: TS map considering $E > 500$ MeV photons during a short-flare episode at MET: 296164808-298860398. Black dashed lines representing 68% and 95% containment region for the γ -ray signature. Top right: The corresponding SED of this object. Bottom: Light curve for 5BZQJ 0010+1058 background extracted with likelihood analysis; flux points are calculated only for bins having $TS > 4$ with a 30 day time bin along 7.5 yrs of observations, integrating 0.3-500 GeV photons.

tect by means of a dedicated study focusing on blazars as γ -ray candidates.

NGC1052; 5BZUJ 0241-0815. In this case, the light curve shows a flaring state during 2013 to first quarter of 2014. From March 7 to April 7, 2014 the γ -ray signature reaches its highest state, at which $TS \approx 12$. A TS map at $E > 500$ MeV (fig. 13) shows that 5BZUJ 0241-0815 is within the 68% confinement region for the γ -ray signature. This blazar of unknown type is another example of a transient γ -ray emitter, which may contribute to building the currently unresolved γ -ray background. It is still not clear how to evaluate the impact of such sources for the observed extragalactic diffuse γ -ray component given that transient populations are not yet fully characterized.

5BZQJ 2136+0041. This source is classified as a FSRQ with $z=1.941$, and for this case we detected a short-lived γ -ray flare from January 2 to February 2, 2014, where $TS \approx 7.5$. A TS map integrating over $E > 300$ MeV photons (Fig. 14, top left) shows that the signature emerges as a point-like source and the 68% containment region is compatible with 5BZQ J2136+0041 position. Although the γ -ray signature has low significance, it is important to report it as a potential faint γ -ray transient. Since we integrated along short time period, the lower limits computed in the γ -ray SED (Fig. 14, top right) are not so restrictive.

From the three cases presented in this section, two questions clearly arise: How many AGNs could have short-lived flares, and how important is their integrated contribution to the γ -ray background probed by Fermi-LAT (Ackermann et al. 2015a) in the 100 MeV to 800 GeV energy range?

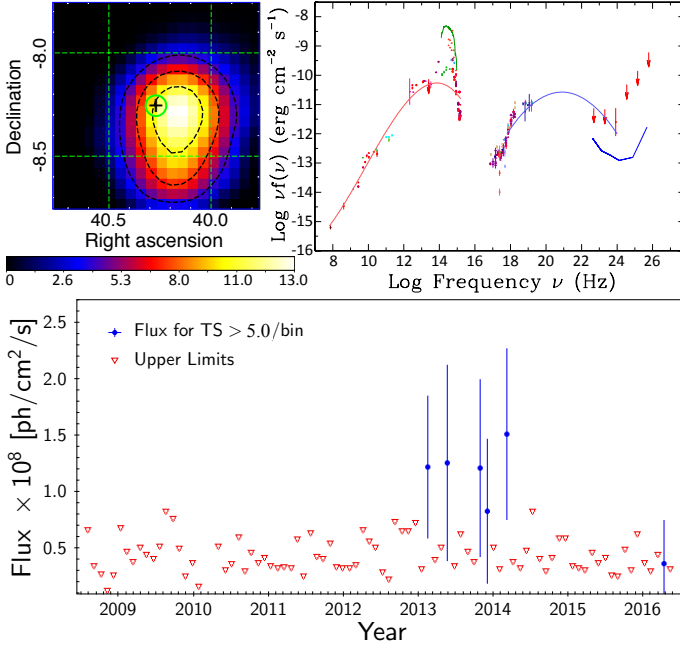


Fig. 13. 5BZUJ 0241-0815. Top left: TS map for $E > 500$ MeV during a short-flare episode at MET: 415846402-418598890. The blazar position is highlighted by the green circle center at “+”; the black dashed-lines are TS surfaces corresponding 68%, 95%, and 99% confinement region for the γ -ray signature. Top right: The corresponding SED of this object; the green template corresponds to the elliptical galaxy emission at $z=0.005$. Bottom: Light curve for 5BZUJ 0241-0815. Flux points are only calculated for bins with $TS > 5$ with a 30 day time bin along 7.5 yrs of observations, integrating 0.3-500 GeV photons.

4.6. Fermi-LAT nondetections

We report on four Radio-Planck sources (5BZQJ 0927+3902, 5BZQJ 2139+1423, 5BZQJ 2022+6136 and 5BZQJ 2007+4029) for which we could not find evidence of γ -ray signature during the 7.5 years of observations.

5BZQJ 0927+3902. This is a bright radio blazar ($z=0.695$) about 46.1 arcminutes away from 3FGL J0923.1+3853 (which is associated to B2 0920+39). We investigate this region with a TS map, looking for signs of source confusion, but we could find none. The 3FGL γ -ray signature dominates the emission in this region as seen by the low-energy TS map (Fig. 15, left); the SED for 5BZQJ 0927+3902 (Fig. 15, right) has no of γ -ray information. This is likely a good proxy for blazars with an IC component that is MeV peaked just as the following cases: 5BZQJ 2139+1423, 5BZQJ 2022+6136, and 5BZQJ 2007+4029.

5BZQJ 2139+1423. This blazar is classified as FSRQ, with relatively high redshift, $z=2.427$. A light curve with one month bins along 7.5 year showed no bins with $TS > 3.0$. However, we do not discard γ -ray activity for this source. The IC component probably peaks at a frequency that is much lower than the bandwidth probed by Fermi-LAT, owing to its LSP frequency $\log(\nu_{peak}) \approx 11.0$. In addition, because of its high redshift, the observed IC end tail gets even harder to probe.

5BZQJ 2022+6136. This source is also classified as FSRQ, although there is no good fitting between the optical

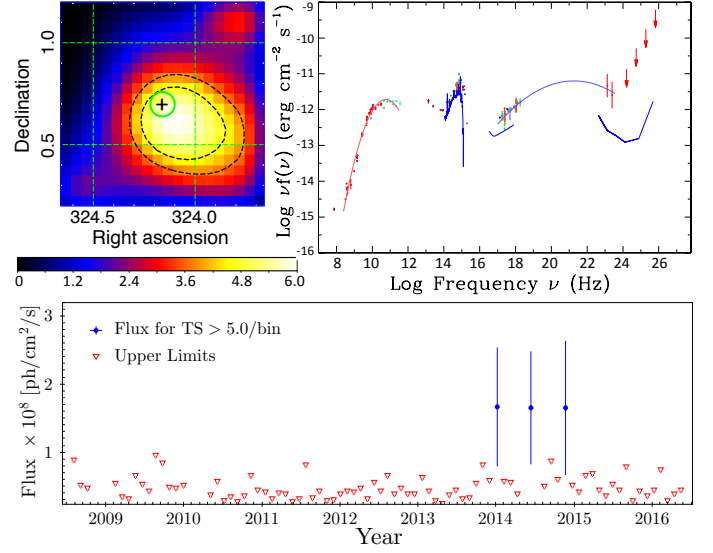


Fig. 14. 5BZQJ 2136+0041. Top left: TS map for $E > 300$ MeV during a short-flare episode at MET: 410341424 413093913. The blazar position is highlighted by a green circle with center at “+”. The black dashed lines correspond to 50% and 68% confinement radius for the γ -ray signature. Top right: The corresponding SED of this object; the blue bump template assumes $z=1.941$. Bottom: Light curve for 5BZQJ 2136+0041, flux is calculated only for $TS > 5$ bins, with a 30 day time bin along 7.5 yrs of observations, integrating 0.3-500 GeV photons.

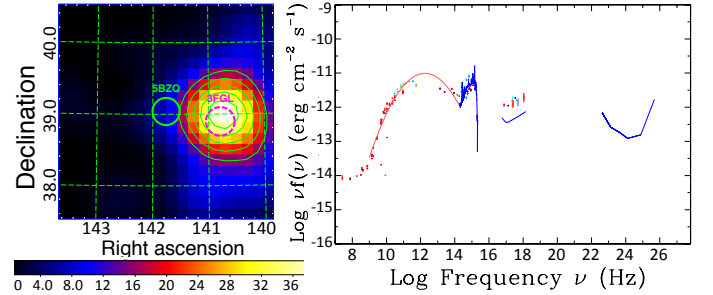


Fig. 15. 5BZQJ 0927+3902. Left: TS map for 750-950 MeV photons. The blazar 5BZQJ 0927+3902 is highlighted as a green circle and 3FGL is shown in magenta. Right: The SED with a polynomial fit to the mean Syn and the blue-bump template are represented for $z=0.695$. In the γ -ray band, the blue curve in the 10^{22} - 10^{26} Hz band (0.1-500 GeV) represents the Fermi-LAT four year sensitivity threshold, therefore an upper limit for the γ -ray emission.

to X-ray data and a blue-bump template (with $z=0.228$). There is a single episode from 27 September to 28 October 2011 for which a low significance γ -ray signal ($TS=4.1$) is present.

5BZQJ 2007+4029. This object is close to the Galactic plane, at latitude $b=4.30^\circ$, with relatively high redshift, i.e., $z=1.736$. A likelihood analysis integrating over 7.5 years, considering the full energy band 0.1-500 GeV shows a very low-significance γ -ray signature, where $TS \approx 5.2$, $\Gamma = 2.61 \pm 0.26$, and $N_0 = 2.4 \pm 1.2 \times 10^{13}$ ph/cm²/s/MeV. However, from the TS map (300 MeV-10 GeV) there is no clear evidence for a point source, therefore we do not consider this as detection.

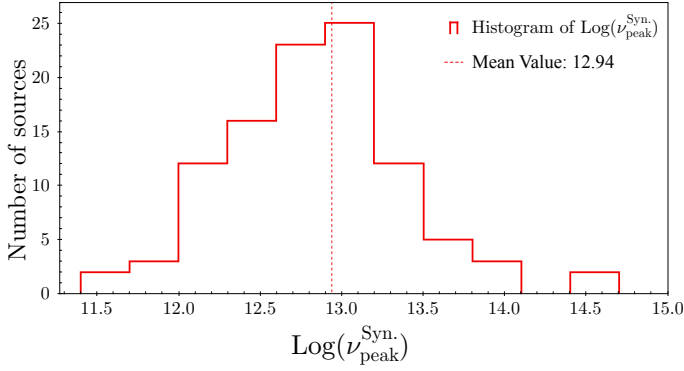


Fig. 16. Distribution of $\log(\nu_{peak}^{Syn})$ [Hz] for the Radio-Planck sample considering all 104 objects, bin size of 0.3; the mean value of $10^{12.94}$ Hz is shown as a dashed line.

5. Radio-Planck sample properties

In previous sections, we showed that 99 of the 104 objects in the Radio-Planck sample have evidence for γ -ray emission at relevant level when integrating over 7.5 years of observation or during flaring episodes. By fitting the Syn and IC components with a third order polynomial (Giommi et al. 2012b), we estimate their SED peak parameters (Table 5) using all available nonsimultaneous data. In particular, the γ -ray points are from the 3FGL catalog in the case of previously detected sources, and from our own data reduction in the case of newly detected sources, considering 7.5 years of Fermi-LAT observations; we also study statistical properties related to the nonthermal peak parameters.

5.1. Synchrotron and IC peak parameters

In Fig. 16 we plot the distribution of $\log(\nu_{peak}^{Syn})$, showing that the Radio-Planck sample is dominated by LSP blazars, with mean value $\langle \log(\nu_{peak}^{Syn}) \rangle = 12.94 \pm 0.07^6$ [Hz]. This is because our sample is flux limited in the microwave band where blazars of the LSP type are by far the most abundant objects.

In Fig. 17 we plot a histogram showing the distribution of $\log(\nu f_\nu)$ peak values for both Syn and IC bumps. A parametric Kolmogorov Smirnov (KS) test comparing both histograms gives a $p_{value} = 0.86$, implying that the luminosity distributions of both components are similar. In fact, the mean values of the peak fluxes are relatively close, i.e., $\langle \log(\nu f_\nu^{Syn}) \rangle = -11.11 \pm 0.05$ [erg/cm²/s]; $\langle \log(\nu f_\nu^{IC}) \rangle = -10.94 \pm 0.05$ [erg/cm²/s]. This similarity in the peak power distribution of the two components suggests that on average the ratio of νf_ν^{Syn} to νf_ν^{IC} values might be close to one for the population of LSP blazars.

5.2. Peak ratio parameter

The ν_{peak}^{Syn} and ν_{peak}^{IC} parameters, which are determined in the $\log(\nu f_\nu)$ versus $\log(\nu)$ plane, are very representative of blazar SED properties because they give the peak energy where most of the Syn and IC power are emitted. To study their statistical properties we define the

⁶ From here on, the errors to the mean values are calculated as σ/\sqrt{n} , where σ is the standard deviation and n is the total number of objects in each sample (or subsample).

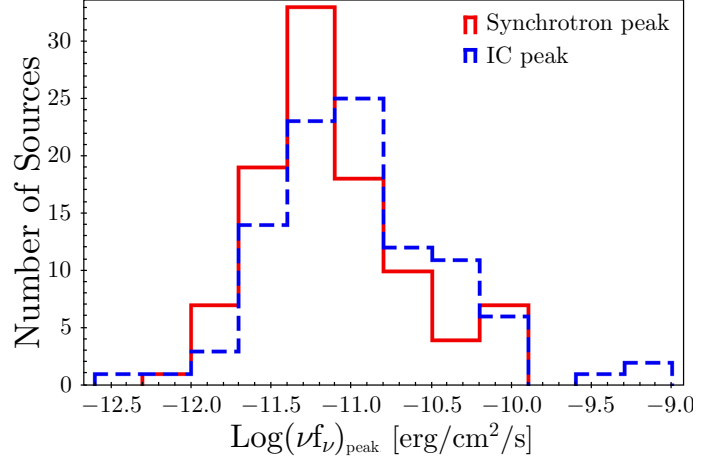


Fig. 17. Histogram of $\log(\nu f_\nu)$ at the Syn peak (in red) and the IC peak (in blue), considering all 99 sources in the Radio-Planck sample for which we could estimate the Syn and IC peak parameters.

peak ratio (PR) parameter as the logarithm of ν_{peak} ratios: $PR = \log(\nu_{peak}^{IC}/\nu_{peak}^{Syn})$ and plot its distribution (Fig. 18). We determine the characteristic mean value for PR when considering all LSP blazars: $\langle PR_{all} \rangle = 8.60 \pm 0.09$. We also show the distribution of PR values for the subsamples classified as 5BZB (BL Lacs), where the mean value $\langle PR_{BL\ Lacs} \rangle = 8.42 \pm 0.20$ and 5BZQs (FSRQ), where the mean value $\langle PR_{FSRQ} \rangle = 8.75 \pm 0.09$. There are no significant differences for the average PR parameters, since variations are contained within errors.

In Fig. 19 we show the $\log(\nu_{peak}^{IC})$ distribution for all 98 LSPs with available IC data (in blue), which has mean value of $\langle \log(\nu_{IC}) \rangle = 21.53 \pm 0.90$ [Hz]. We then use the $\langle PR_{all} \rangle$ value to estimate ν_{peak}^{IC} based on the ν_{peak}^{Syn} according to $\log(\nu_{peak}^{IC}) = \log(\nu_{peak}^{Syn}) + \langle PR_{all} \rangle$. The distribution of ν_{peak}^{IC} calculated via $\langle PR_{all} \rangle$ parameter is shown in pink, which is indeed well described by this simple relation. Most likely, there is a dominant process connecting Syn and IC bumps, otherwise such correlations would not show up. If multiple emission scenarios were at work, we would expect large spreading in the parameter space, not tight Gaussian distributions. As known, the most established picture to describe the SED shape assumes dominant SSC leptonic scenario, but there is extensive discussion in the literature considering the role of the EC for different blazars, even reporting on observable evidence (Meyer et al. 2012).

A scatter plot with $\log(\nu_{IC})$ values versus $\log(\nu_{Syn}) + \langle PR_{all} \rangle$ shows that there is only marginal evidence for the correlation between those parameter (Fig. 19, bottom) given that the Pearson's correlation coefficient r for a linear fit is ~ 0.17 . The fact that the PR parameter helped to describe the distribution of $\log(\nu_{IC})$ as a population, tells us that the $\log(\nu_{IC})$ measured by our fitting might have large uncertainties; given the absence of a significant correlation, when comparing case by case with the scatter plot. Indeed there is a large uncertainty for that parameter mainly due to the huge data gap in the energy window between tens of KeV up to hundreds of MeV, which is smoothed out when considering the whole population of bright LSP sources.

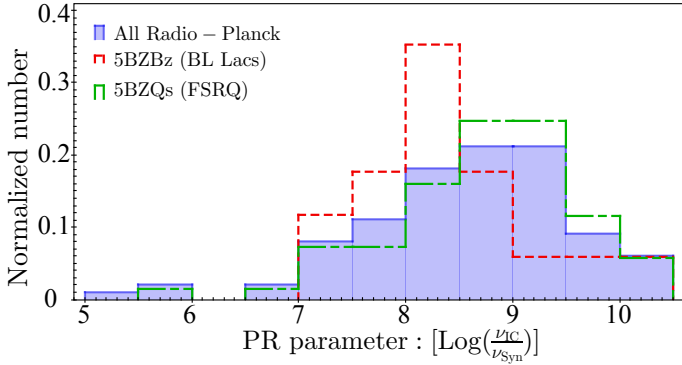


Fig. 18. Peak ratio $\log(\nu_{\text{peak}}^{\text{IC}}/\nu_{\text{peak}}^{\text{Syn}})$ distribution. Full indigo bars represent the whole Radio-Planck sample, red dashed bars indicated the subsample of BL Lacs, and green dot-dashed bars show the subsample of FSRQ.

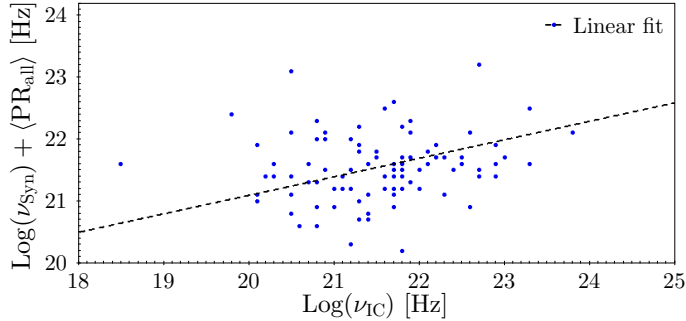
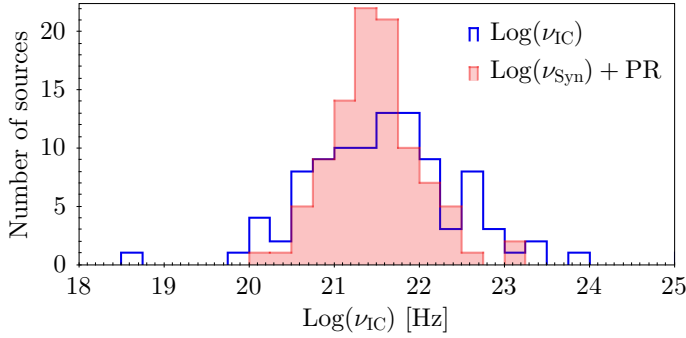


Fig. 19. Top: Distribution of $\log(\nu_{\text{peak}}^{\text{IC}})$ in blue, using measured values from fitting the IC component, and in pink using $\log(\nu_{\text{peak}}^{\text{IC}}) = \log(\nu_{\text{peak}}^{\text{Syn}}) + \langle \text{PR}_{\text{all}} \rangle$ to estimate ν^{IC} based on ν^{Syn} measurements. Bottom: A scatter plot with $\log(\nu_{\text{IC}})$ values vs. $\log(\nu_{\text{Syn}}) + \langle \text{PR}_{\text{all}} \rangle$ together with a linear fit showing weak correlation.

5.3. Compton dominance

The ratio of IC to Syn peak power is known as the Compton dominance (CD). This is an important parameter for describing blazar SEDs (Finke 2013; Potter & Cotter 2013; Nalewajko & Gupta 2017), since it measures the dominant power output component for each source, i.e.,

$$\text{CD} = \frac{L_{\text{IC}}}{L_{\text{Syn}}} \equiv \frac{\nu f_{\nu}^{\text{IC}}}{\nu f_{\nu}^{\text{Syn}}}; \text{ at the SED peaks.} \quad (2)$$

Luminosity is written as $L = 4\pi d_L^2 \nu f_{\nu} / (1+z)^{1-\alpha}$, where d_L represents the luminosity distance and the $(1+z)^{1-\alpha}$ factor is the k-correction assuming a power-law spectrum with energy index α . Since we calculate the CD using the

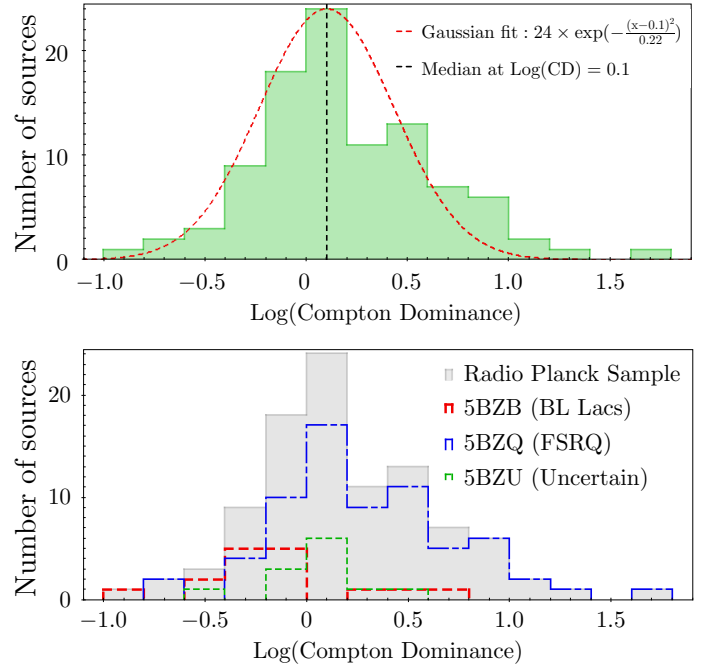


Fig. 20. Log(CD) distribution for the Radio-Planck sample. Top: The green bars represent all 99 cases that have Syn + IC data available for calculating the CD parameter. The red dashed line represents a Gaussian function with $\sigma^2=0.22$ around the median value of $\log(\text{CD})=0.1$. Bottom: The log(CD) distribution for BL Lacs (red dashed lines), FSRQ (blue dot-dashed lines), and blazars classified as uncertain are shown in green dashed lines.

luminosity ratio at the peak power, $\alpha=1$ for both IC and Syn peaks, and the luminosity ratio is simply the flux ratio.

In Fig. 20 (top) we plot in green the distribution of $\log(\text{CD})$ parameter for the Radio-Planck sample, which has a median value of 0.1. The median is only slightly larger than 0, implying that on average, the peak-power output for the sync and IC components are similar. In Fig. 20 (top), we add a tentative Gaussian fit to the $\log(\text{CD})$ distributions, showing that a single Gaussian function (red dashed line) hardly describes the overall shape, particularly the highest CD values. The tail toward $\log(\text{CD}) > 1.0$ probably owing to strong variability in γ -rays compared to radio bands, pushing $\log(\text{CD})$ to high values. The mean value $\langle \log(\text{CD}) \rangle = 0.17 \pm 0.05$ is clearly affected by that, therefore a median might be more reliable as the representation of steady γ -ray activity in LSP blazars.

The histograms at bottom panel of Fig. 20 represent the CD for different subsamples defined according to the 5BZcat classification, that is, BL Lacs, FSRQ, and unclassified sources. Nalewajko & Gupta (2017) have also estimated the CD for FSRQ and BL Lacs, but based on luminosities at fixed energies: $L_{(1 \text{ GeV})}$ as measured with Fermi-LAT, and $L_{(3.4 \mu\text{m})}$ as measured with the W1 channel from WISE satellite, for instance, $\text{CD} = L_{(1 \text{ GeV})}/L_{(3.4 \mu\text{m})}$. Our measurements instead are taken at the peak of Syn and IC components. In both cases, there is a trend for BL Lacs to populate the $\log(\text{CD})$ range with the lowest values (with mean $\langle \log(\text{CD}) \rangle_{(\text{BL-Lac})} = -0.16 \pm 0.08$), while FSRQ populate a wider region (with mean $\langle \log(\text{CD}) \rangle_{(\text{FSRQ})} = 0.28 \pm 0.06$ for the Radio-Planck sample). We also checked whether the

$\log(\text{CD})$ distribution depends on radio flux density splitting the sample in two subsets with $f_{5\text{GHz}} > 1.5$ Jy and ≤ 1.5 Jy, at 5 GHz. As result, the two histograms turned out to be very similar (a KS test gives a p-value = 0.693). Also a scatter plot of radio flux versus $\log(\text{CD})$ shows no evidence of correlation between these quantities.

In Fig. 21 we plot the CD versus IC peak energy (E_{IC} , in MeV). When considering the whole sample, there is no clear correlation between those parameters (the Pearson's correlation coefficient $r \approx 0.13$). However for individual classes (BL Lacs, FSRQ, and uncertain types) the BL Lacs tend to be associated with the highest IC peak energies, even though they are not dominating the end tail with high $\log(\text{CD})$ values (Fig. 20, bottom).

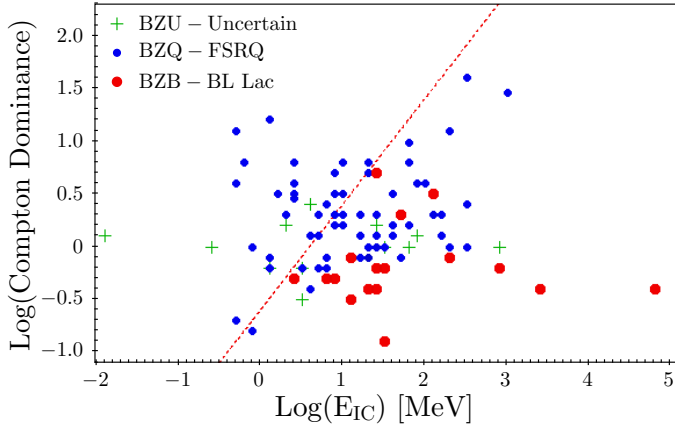


Fig. 21. Compton dominance vs. energy associated with the IC peak (E_{IC}) for the Radio-Planck sample. We plot FSRQs as blue dots, BL Lacs as red dots, and uncertain blazars as green crosses. The red dotted line sets a qualitative cut to highlight the region populated by BL Lacs.

5.4. Influence of variability on the Compton dominance

According to Acero et al. (2015) the variability index indicates if a γ -ray source is variable on a timescale of months, not addressing shorter or longer time variations. An index > 72.4 indicates a $> 99\%$ confidence probability that the source is variable. At least $\approx 2/3$ of the Radio-Planck sources (66 out of 104) have a variability index > 72.4 therefore detected as variables on a timescale of months. To investigate if the variability index could be correlated to the CD, we plot in Fig. 22 the γ -ray $\log(\text{Var.index})$ taken from the 3FGL catalog versus our estimate of the parameter $\log(\text{CD})$. A linear fit of the scatter plot (Fig. 22) has a Pearson correlation coefficient of 0.40, meaning the positive correlation between $\log(\text{Var.index})$ and $\log(\text{CD})$ is relatively weak. In fact, this only tells us that the variability index might not be the best parameter to rely on if we are willing to investigate the influence of γ -ray variability over the CD parameter.

Looking at individual cases however provides a better picture of CD variations induced by fast variability. We consider first the three sources detected in γ -rays only during flaring episodes (Sec. 4.5). These objects move from $\log(\text{CD}) < -1.0$ (during γ -ray quiet period) up to 0.79, 0.31, and 2.51, respectively, for BZQJ 0010+1058, BZUJ 0241-

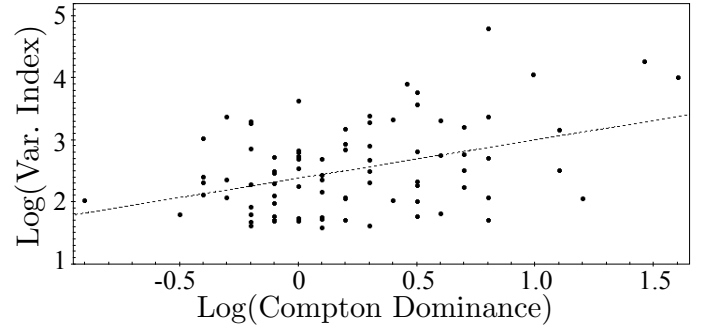


Fig. 22. γ -ray variability index vs. $\log(\text{CD})$ for the Radio-Planck sample. The dashed line represents a linear fit $\log(\text{variability Index}) = m \times \log(\text{CD}) + k$, where the constants are $m = 0.618$ and $k = 2.39$.

0815, and BZQJ 2136+0041, and all cases show variability on timescales at least lower than one month (given that they are detected within isolated month bins), i.e., shorter than the monthly time bin described by the variability index parameter. Further studies are necessary to investigate the dependencies of transient and fast flares with respect to a time-bin smaller than that of a month, which we used.

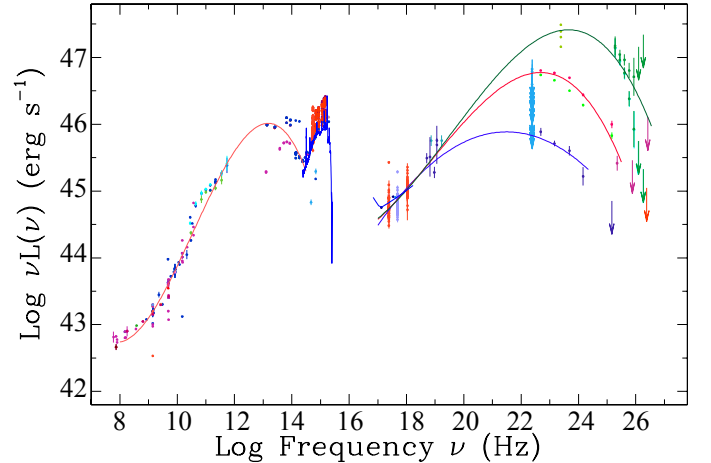


Fig. 23. SED for BZQJ 1224+2122, with blue bump template assuming $z = 0.434$. This source has the largest γ -ray variability index, and we fit the IC component during various flaring states. In the high-energy band, the blue line refers to the 1FGL detection (integrating 2008-2009 data), the red line refers to the 3FGL detection (2008-2012 data), and the dark-green line represents a short and relatively bright flare reported by the MAGIC team Aleksić et al. (2011) with reported variability within few hours.

Another example of strong γ -ray variability is BZQJ 1224+2122 (4C+21.35), whose SED is shown in Fig. 23. We fit both Syn and IC components with a third order polynomial, listing fit parameters and their corresponding CD values in table 4. We note that the high-energy peak flux changes by one order of magnitude in between 1FGL (dark blue) and 2FGL catalogs (red). This kind of long timescale variability (several months) is well represented by the variability index. When checking the light curve

available online⁷ we see that this source had a relatively steady γ -ray emission during the first year of observations by Fermi-LAT (08/2008 to 08/2009, corresponding to the 1FGL SED; dark blue points), while it later underwent a strong activity when the photon flux varied by more than one order of magnitude in the 0.1-500 GeV band.

Since a more active state appears just after the integration time used for building the 1FGL catalog, we know that the flaring activity is now smoothed over two and four years of integration time. These integration times are used for the 2FGL and 3FGL catalogs represented by red and light green points, respectively, in the high-energy SED. However, when integrating data only during the brightest state, it is possible to observe $E > 100$ GeV flux variability of \approx one order of magnitude within hourly timescale, as for the flaring episode reported by Aleksić et al. (2011). This is a clear example of how the $\log(\text{CD})$ parameter can vary widely, from -0.2 (during steady γ -ray emission) to $+0.6$ (when integrating over steady+flaring states), and reaching up to $+1.3$ (at the peak-flaring) as reported in Table 4.

Table 4. Inverse Compton peak parameters in various flaring states for 5BZQJ 1224+2122. First to last line in table correspond to blue, red, and green curves, respectively, from Fig. 23.

Epoch	$\log(\nu_{IC}^{peak})$	$\log(\nu f_\nu)$	$\log(\text{CD})$
1FGL	21.5	-10.9	-0.2
3FGL	22.7	-10.1	+0.6
Flare	23.6	-9.40	+1.3

Overall, these examples suggest that γ -ray flaring states are likely to generate the largest CD values in the tail of the distribution (Fig. 20, top). During flare episodes, the sources could be moving from a nearly steady multicomponent SSC + EC regime, to a short-lived EC-dominated regime, which produce large amplitude variability (up to three orders of magnitude) owing to the extra beaming factor $\propto \delta^{1-\alpha}$ Dermer (1995) that is present in EC scenario. We will investigate that in a forthcoming paper.

5.5. Compton dominance versus ν_{peak}^{Syn} plane

Here we report on the relation between $\log(\text{CD})$ and $\log(\nu_{peak}^{Syn})$ that has been argued in literature (Fossati et al. 1998; Nalewajko & Gupta 2017; Potter & Cotter 2013) to show a relatively strong correlation. In fact, for our sample the Pearson’s correlation coefficient r between $\log(\text{CD})$ and $\log(\nu_{peak}^{Syn})$ is very weak, $r \sim -0.336$, a direct consequence of the large scatter associated with these parameters. As shown in figure 24, we cover almost three decades in ν_{peak} space, suggesting that the correlation between $\log(\text{CD})$ and $\log(\nu_{peak}^{Syn})$ parameters should be considered with great care in order to evaluate its dependence on selection effects when building the study sample.

It is also important to keep in mind that CD estimates reported for blazars with $\log(\nu_{peak}) > 15.0$ are rather uncertain and subject to strong selection effects. It is extensively

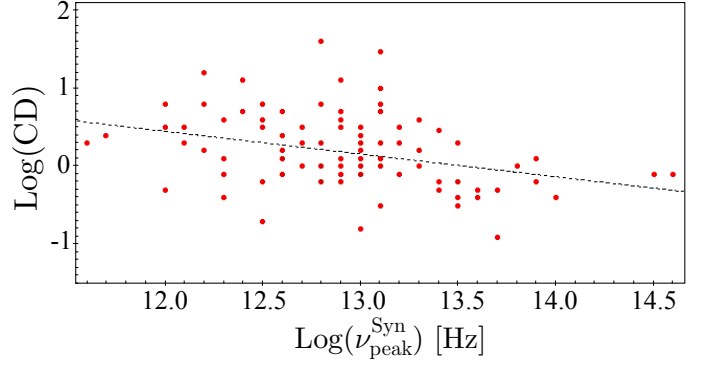


Fig. 24. $\log(\text{CD})$ vs. $\log(\nu_{peak}^{Syn})$ plane for the Radio-Planck sample, probing almost three orders of magnitude in ν_{peak}^{Syn} space and showing very weak correlation with a large scatter. The black dashed line is a linear fit $\log(\text{CD}) = -0.29 \log(\nu_{peak}^{Syn}) + 3.92$.

mentioned in literature (Acero et al. 2015; Ackermann et al. 2015b; Arsioli et al. 2015; Chang et al. 2017) that HSP blazars on average have a hard γ -ray spectral slope with $\langle \Gamma \rangle$ ranging from 1.8 to 2.0, and therefore the IC peak is most of the times out of reach for the Fermi-LAT, given its sensitivity window. For the brightest cases in which the IC peak was probed by VHE Cherenkov observatories, there is still the uncertainty introduced by absorption of VHE photons due to pair creation when scattering EBL photons. Indeed, only a few HSP sources have their IC peak probed by VHE observatories with observations triggered by X-ray and γ -ray flaring states. This alone introduces a strong bias, given that no VHE blind sky survey is available.

6. Conclusions

The Radio-Planck sample includes 104 bright radio-selected sources ($f > 1$ Jy at 37 GHz), 102 of which are optically identified blazars in the 5BZcat and were expected to be detected by the Fermi-LAT. The two remaining objects are radio galaxies, namely 3C111 and M87, both detected in γ -rays. The noninclusion of a fair fraction of 5BZcat sources in published Fermi-LAT catalogs motivated our search for new γ -ray detections using 7.5 years of data as available at the time of writing. The main results of our work can be summarized as follows. Out of 104 sources, 83 have counterparts from FGL catalogs (all $\text{TS} > 25$); 6 are new detections with $\text{TS} > 20$; 3 are new detections with TS in between 10 to 20; 3 are new associations with 3FGL sources (from improved positioning with high-energy TS maps); 1 is a new detection from solving γ -ray source-confusion; and 3 are transients that were detected during short flaring episodes.

Five sources remain undetected in the γ -ray band, all of which are optically identified blazars included in the 5BZcat. Two objects have relatively high redshift (5BZQJ 2139+1423 at $z = 2.427$ and 5BZQJ 2007+4029 at $z = 1.736$). The remaining three sources are 5BZQJ 0927+3902 ($z = 0.695$), 5BZQJ 2022+6136 ($z = 0.228$), 5BZQJ 1927+7358 ($z = 0.302$).

We conclude that most of sources currently called γ -ray quiet blazars are actually associated with relevant γ -ray signatures, becoming evident by means of a dedicated case-by-case study of 7.5 yr of Fermi-LAT observations. At most, γ -

⁷ Light curve for BZQJ 1224+2122 (3FGLJ 1224.9+2122): http://fermi.gsfc.nasa.gov/ssc/data/access/lat/4yr_catalog/ap_1cs/lightcurve_3FGLJ1224.9p2122.png

ray quiet blazars might be a very small fraction of the LSP population, suggesting there is no urgent need to introduce a new blazar class. From the five nondetections reported, two are high redshift sources, where absorption may hinder a γ -ray signature. Another case (5BZQJ 0927+3902) is associated with a bright 3FGL source that dominates the region, such that we could not probe for source confusion. Finally, 5BZQJ 2022+6136 and 5BZQJ 1927+7358 only showed hints of flaring activity and are probably under Fermi-LAT sensitivity.

All new detections reported in this work contribute to solve a small fraction of the extragalactic γ -ray background into point-like sources. We note that the presence of transient sources, which are only detectable during short flaring episodes, could represent a non-negligible fraction of the MeV to GeV background. This would be a possible approach to consider in future studies. We discuss examples of how to extract refined and relevant γ -ray information by considering a multifrequency approach when searching for new sources, showing that Fermi-LAT database is a large resource still to be explored in detail.

We study the CD distribution, showing that a single Gaussian function fails to describe the cases with large $\log(\text{CD})$ values at the tail of the histogram. There is indeed a number of high $\log(\text{CD})$ sources that are in excess with respect to a single Gaussian fitting. We evaluate the impact of fast γ -ray variability on the CD parameter, considering 5BZQJ 1224+2122 as an example. We point out three cases in which large CD values are observed during fast flaring states (BZQJ 0010+1058, BZUJ 0241-0815, and BZQJ 2136+0041), such that CD values can be one to two orders of magnitude larger compared to those obtained during the steady and relatively faint γ -ray emission. As follows, the absent correlation between $\log(\text{CD})$ versus $\log(\text{Var. Index})$ in the scatter plot from Fig. 22 shows that the γ -ray variability index may not be the best tool to evaluate the relation connecting γ -ray flaring states and large $\log(\text{CD})$ sources. Finally, we also evaluate the putative correlation between $\log(\text{CD})$ and $\log(\nu_{\text{peak}}^{\text{Syn}})$ parameters, finding relatively weak evidence for that. The similarity between Syn and IC ν_f peak distributions and the tight peak ratio $\log(\nu_{\text{peak}}^{\text{IC}}/\nu_{\text{peak}}^{\text{Syn}})$ distribution points to a dominant mechanism (either SSC or EC) to account for the IC component in bright LSP blazars, otherwise we would have found a large spread in the parameter space we probed. An extensive evaluation testing SSC and EC scenarios is explored with great detail in a parallel work (Arsioli & Chang 2018), which is based on the Radio-Planck sample.

Also, we showed a few examples for which the power-law fitting parameters estimated for faint γ -ray blazars, which were detected with TS between 10 to 25 under 3FGL setup integrating over 4.0 years of Pass7 data, are later confirmed when integrating over a larger exposure time of 7.5 years. This vindicates the importance and usefulness of reporting faint γ -ray signatures in association with blazar counterparts.

Acknowledgements. During this work, BA was supported by the Brazilian Scientific Program Ciências sem Fronteiras - Cnpq, and later by São Paulo Research Foundation (FAPESP) with grant n. 2017/00517-4. We would like to thank Prof. Paolo Giommi for his comments along the preparation of this work, Prof. Marcelo M. Guzzo and Prof. Orlando L. G. Peres for the full support which allowed the author partnership with FAPESP. We thanks IcrANet and Prof. Carlo Bianco for the cooperation granting access to Joshua Computer

Cluster (Rome-Italy) for Fermi-LAT data reduction. We thank the CCJDR Data Center at IFGW Unicamp (Campinas-Brazil) where we also performed Fermi-LAT data reduction at their Feynman Cluster. We thank SSDC, Space Science Data Center from Agenzia Spaziale Italiana; University La Sapienza of Rome, Department of Physics; And State University of Campinas - Unicamp, IFGW Department of Physics for hosting the author. We make use of archival data and bibliographic information obtained from the NASA-IPAC Extragalactic Database (NED), data, and software facilities from the SSDC.

References

- Abdo, A. A., Ackermann, M., Agudo, I., et al. 2010, *ApJ*, 716, 30
 Abdo, A. A., Ackermann, M., Ajello, M., et al. 2010, *The Astrophysical Journal Supplement Series*, 188, 405
 Acero, F., Ackermann, M., Ajello, M., et al. 2015, *ApJS*, 218, 23
 Acero, F., Donato, D., Ojha, R., et al. 2013, *ApJ*, 779, 133
 Ackermann, M., Ajello, M., Albert, A., et al. 2013, *ApJ*, 771, 57
 Ackermann, M., Ajello, M., Albert, A., et al. 2015a, *ApJ*, 799, 86
 Ackermann, M., Ajello, M., Albert, A., et al. 2016a, *Physical Review Letters*, 116, 151105
 Ackermann, M., Ajello, M., Albert, A., et al. 2012, *Phys. Rev. D*, 85, 083007
 Ackermann, M., Ajello, M., Allafort, A., Antolini, E., & Atwood, e. a. 2011, *ApJ*, 743, 171
 Ackermann, M., Ajello, M., Atwood, W. B., & Baldini, e. a. 2015b, *ApJ*, 810, 14
 Ackermann, M., Ajello, M., Atwood, W. B., et al. 2016b, *ApJS*, 222, 5
 Ajello, M., Atwood, W. B., Baldini, L., et al. 2017, *ApJS*, 232, 18
 Aleksić, J., Antonelli, L. A., Antoranz, P., et al. 2011, *ApJ*, 730, L8
 Ando, S., Benoit-Lévy, A., & Komatsu, E. 2014, *Phys. Rev. D*, 90, 023514
 Angelakis, E., Hovatta, T., Blinov, D., et al. 2016, *MNRAS*, 463, 3365
 Arsioli, B. & Chang, Y.-L. 2017, *A&A*, 598, A134
 Arsioli, B. & Chang, Y.-L. 2018, *Accepted for publication, April 9 2018, A&A, Ref. number: AA/2018/33005*
 Arsioli, B., Fraga, B., Giommi, P., Padovani, P., & Marrese, P. M. 2015, *A&A*, 579, A34
 Atwood, W., Albert, A., Baldini, L., et al. 2013, *ArXiv e-prints*
 Atwood, W. B., Abdo, A. A., Ackermann, M., et al. 2009, *ApJ*, 697, 1071
 Blinov, D., Pavlidou, V., Papadakis, I., et al. 2015, *MNRAS*, 453, 1669
 Chang, Y.-L., Arsioli, B., Giommi, P., & Padovani, P. 2017, *A&A*, 598, A17
 Condon, J. J., Cotton, W. D., Greisen, E. W., et al. 1998, *AJ*, 115, 1693
 Cuoco, A., Komatsu, E., & Siegal-Gaskins, J. M. 2012, *Phys. Rev. D*, 86, 063004
 De Angelis, A., Tatischeff, V., Grenier, I. A., et al. 2017, *ArXiv e-prints*
 Dermer, C. D. 1995, *ApJ*, 446, L63
 Di Mauro, M. & Donato, F. 2015, *Phys. Rev. D*, 91, 123001
 Di Mauro, M., Donato, F., Lamanna, G., Sanchez, D. A., & Serpico, P. D. 2014, *ApJ*, 786, 129
 Finke, J. D. 2013, *The Astrophysical Journal*, 763, 134
 Fornasa, M. & Sánchez-Conde, M. A. 2015, *Phys. Rep.*, 598, 1
 Fossati, G., Maraschi, L., Celotti, A., Comastri, A., & Ghisellini, G. 1998, *MNRAS*, 299, 433
 Franceschini, A., Rodighiero, G., & Vaccari, M. 2008, *A&A*, 487, 837
 Giommi, P., Padovani, P., Polenta, G., et al. 2012a, *MNRAS*, 420, 2899
 Giommi, P., Polenta, G., Lähteenmäki, A., et al. 2012b, *A&A*, 541, A160
 Gregory, P. C., Scott, W. K., Douglas, K., & Condon, J. J. 1996, *ApJS*, 103, 427
 Grupe, D., Komossa, S., Leighly, K. M., & Page, K. L. 2010, *ApJS*, 187, 64
 Inoue, Y. 2014, *Fifth Fermi Symposium Proceedings, Nagoya, Japan*.
 Lister, M. L., Aller, M. F., Aller, H. D., et al. 2015, *ApJ*, 810, L9
 Lister, M. L., Homan, D. C., Kadler, M., et al. 2009, *ApJ*, 696, L22
 MacDonald, N. R., Jorstad, S. G., & Marscher, A. P. 2017, *ApJ*, 850, 87
 Massaro, E., Maselli, A., Leto, C., et al. 2015, *Astrophysics and Space Science*, 357

- Mattor, J. R., Bertsch, D. L., Chiang, J., et al. 1996, ApJ, 461, 396*
Meyer, E. T., Fossati, G., Georganopoulos, M., & Lister, M. L. 2012, The Astrophysical Journal Letters, 752, L4
Nalewajko, K. & Gupta, M. 2017, A&A, 606, A44
Padovani, P., Alexander, D. M., Assef, R. J., et al. 2017, A&A Rev., 25, 2
Padovani, P. & Giommi, P. 1995, ApJ, 444, 567
Paliya, V. S., Marcotulli, L., Ajello, M., et al. 2017, ApJ, 851, 33
Planck Collaboration, Aatrokoski, J., Ade, P. A. R., et al. 2011, A&A, 536, A15
Potter, W. J. 2018, MNRAS, 473, 4107
Potter, W. J. & Cotter, G. 2013, Monthly Notices of the Royal Astronomical Society, 431, 1840
Prokhorov, D. A. & Churazov, E. M. 2014, A&A, 567, A93
Tatischeff, V., Tavani, M., von Ballmoos, P., et al. 2016, in Proc. SPIE, Vol. 9905, Space Telescopes and Instrumentation 2016: Ultraviolet to Gamma Ray, 99052N
Vanden Berk, D. E., Richards, G. T., Bauer, A., et al. 2001, AJ, 122, 549

Table 5. Here we list all 104 sources used for our studies. Column 5BZcat shows the blazar name according to Massaro et al. (2015), where BZQ stands for Flat Spectrum Radio Quasars, BZB for BL Lacs and BZU for still undefined-class blazars. Following we list coordinates R.A. and Dec. (J2000) for each source. Columns NVSS shows the radio counterpart according to the NVSS catalog (Condon et al. 1998). Column z corresponds to the redshift as reported in the 5BZcat Massaro et al. (2015), and from the NASA/IPAC Extragalactic Database (NED). Columns $\log(\nu_{\text{peak}}^{\text{Syn}})$ and $\log(\nu_{\text{peak}}^{\text{Syn}})$ are the fitting parameters referring to the peak frequency from Syn and IC components measured in Hz. Columns $\log(\nu f_{\nu}^{\text{Syn}})$ and $\log(\nu f_{\nu}^{\text{IC}})$ correspond to the Syn and IC peak-power measured in $\text{erg}/\text{cm}^2/\text{s}$. All fitting parameters are given as a measure of the mean SED, considering all available data.

5BZcat J	R.A.	Dec.	NVSS J	z	$\log(\nu)$	$\log(\nu f_{\nu})$	$\log(\nu_{\text{IC}})$	$\log(\nu f_{\nu-\text{IC}})$
5BZBJ0050-0929	12.67167	-9.48500	005041-092906	0	14.6	-11.0	22.7	-11.1
5BZQJ1512-0905	228.21056	-9.09995	151250-090600	0.360	13.1	-10.9	22.2	-9.91
5BZQJ2229-0832	337.41705	-8.54847	222940-083254	1.560	13.1	-11.2	21.8	-10.5
5BZQJ0607-0834	91.99875	-8.58056	060759-083450	0.870	12.1	-11.5	21.4	-11.0
5BZUJ0241-0815	40.27000	-8.25576	024104-081521	0.005	13.5	-10.1	20.9(?)	-10.6
5BZQJ0808-0751	122.06473	-7.85275	080815-075109	1.837	13.0	-11.1	22.9	-10.7
5BZQJ0006-0623	1.55791	-6.39333	000613-062335	0.347	13.0	-11.1	20.3	-11.9
5BZQJ1256-0547	194.04652	-5.78931	125611-054720	0.536	12.8	-10.0	22.7	-10.0
5BZQJ2225-0457	336.44693	-4.95039	222547-045701	1.404	13.0	-10.8	21.7	-10.9
5BZQJ2218-0335	334.71683	-3.59358	221852-033537	0.901	12.3	-11.3	21.0	-11.7
5BZQJ1743-0350	265.99527	-3.83461	174358-035004	1.057	12.6	-11.3	21.0	-11.2
5BZBJ2134-0153	323.54294	-1.88812	213410-015317	1.283	12.8	-11.3	21.8	-11.5
5BZQJ0501-0159	75.30338	-1.98729	050112-015912	2.291	13.0	-11.4	21.4	-11.1
5BZQJ0339-0146	54.87891	-1.77667	033930-014635	0.805	12.6	-11.3	22.0	-11.1
5BZQJ0423-0120	65.81583	-1.34253	042315-012032	0.916	13.0	-10.6	22.1	-10.7
5BZUJ0725-0054	111.46125	-0.91556	072550-005458	0.128	13.5	-11.0	20.5	-11.2
5BZQJ0125-0005	21.37017	-0.09889	012528-000556	1.077	12.8	-11.6	20.3	-11.6
5BZQJ2136+0041	324.16080	0.69839	213638+004154	1.941	11.7	-11.6	21.2	-11.2
5BZQJ0108+0135	17.16154	1.58342	010838+013458	2.099	12.9	-11.2	22.4	-10.6
5BZQJ0739+0137	114.82513	1.61794	073918+013704	0.189	13.9	-10.9	21.6	-10.8
5BZUJ1058+0133	164.62338	1.56633	105829+013358	0.890	13.1	-10.9	22.3	-10.8
5BZQJ1229+0203	187.27792	2.05222	122906+020305	0.158	13.4	-10.0	20.8	-9.54
5BZQJ1549+0237	237.37267	2.61700	154929+023700	0.414	12.9	-11.2	22.0	-11.1
5BZBJ0825+0309	126.45958	3.15667	082550+030924	0.506	13.1	-11.1	21.5(?)	-11.6
5BZQJ1222+0413	185.59375	4.22083	122222+041317	0.966	12.7	-11.2	20.8	-10.7
5BZUJ0433+0521	68.29620	5.35433	043311+052115	0.033	13.8	-10.2	19.8	-10.2
5BZQJ2123+0535	320.93549	5.58947	212344+053522	1.941	12.6	-11.7	21.6	-11.8
5BZQJ1038+0512	159.69492	5.20808	103846+051229	0.473	12.0	-11.8	20.8	-12.1
5BZQJ1550+0527	237.64696	5.45290	155035+052710	1.422	13.0	-11.4	21.8	-11.4
5BZQJ2148+0657	327.02252	6.96055	214805+065739	0.999	12.5	-10.8	20.5	-11.0
5BZUJ1751+0939	267.88675	9.65019	175132+093901	0.322	13.1	-10.8	21.9	-10.8
5BZBJ0757+0956	119.27766	9.94303	075706+095634	0.266	13.7	-10.8	20.8	-11.1
5BZQJ0309+1029	47.26500	10.48778	030903+102916	0.863	12.8	-11.2	21.7	-11.2
5BZQJ1608+1029	242.19249	10.48550	160846+102908	1.226	12.8	-11.3	21.6	-11.0
5BZQJ1504+1029	226.10408	10.49417	150425+102938	1.839	12.8	-11.6	22.9	-10.0
5BZQJ0010+1058	2.62917	10.97472	001030+105827	0.089	14.5	-10.7	20.5	-10.8
5BZBJ0449+1121	72.28196	11.35778	044907+112128	2.153	12.9	-11.5	21.8	-10.8
5BZQJ2232+1143	338.15167	11.73055	223236+114350	1.037	12.4	-11.2	21.3	-10.5
5BZQJ0750+1231	117.71687	12.51801	075052+123104	0.889	12.6	-11.1	21.2	-11.2
5BZQJ0530+1331	82.73508	13.53200	053056+133155	2.070	12.2	-11.5	21.4	-10.7
5BZUJ1415+1320	213.99500	13.34000	141558+132024	0.247	12.8	-11.0	20.5	-11.2
5BZQJ2139+1423	324.75546	14.39333	213901+142336	2.427	12.2	-11.7	-	-
5BZUJ0204+1514	31.21004	15.23639	020450+151411	0.833	12.6	-11.6	21.0	-11.2
5BZQJ2253+1608	343.49042	16.14805	225357+160853	0.859	13.1	-10.0	22.2	-9.20
5BZBJ0238+1636	39.66167	16.61639	023838+163658	0.940	13.0	-10.9	22.5	-10.4
5BZQJ2203+1725	330.86203	17.43006	220326+172548	1.076	13.3	-10.9	22.9	-10.9
5BZBJ0738+1742	114.53083	17.70528	073807+174219	0.424	13.5	-10.6	23.8	-11.0
5BZQJ0510+1800	77.50988	18.01155	051002+180041	0.416	13.3	-11.3	21.3	-11.1
5BZBJ0854+2006	133.70332	20.10833	085448+200630	0.306	13.6	-10.4	21.8	-10.8
5BZQJ1224+2122	186.22713	21.37972	122454+212247	0.434	13.1	-10.7	23.0	-10.0
5BZQJ0152+2207	28.07525	22.11881	015218+220707	1.320	12.9	-11.5	21.8	-11.5
5BZQJ1327+2210	201.75359	22.18060	132700+221050	1.398	12.6	-11.7	21.7	-11.0
5BZQJ0830+2410	127.71700	24.18333	083052+241058	0.939	12.6	-11.1	21.8	-11.0
5BZQJ1043+2408	160.78749	24.14306	104309+240835	0.560	12.9	-11.5	21.7	-11.6
5BZQJ0956+2515	149.20784	25.25446	095649+251515	0.712	12.7	-11.4	21.9	-11.4

Table 5. continued.

5BZcat J	R.A.	Dec.	NVSS J	z	$\log(\nu)$	$\log(\nu f_\nu)$	$\log(\nu_{IC})$	$\log(\nu f_{\nu-IC})$
5BZQJ2236+2826	339.09363	28.48261	223622+282858	0.790	13.0	-11.2	22.5	-10.9
5BZQJ0237+2848	39.46838	28.80250	023752+284809	1.206	12.9	-11.2	22.0	-10.7
5BZQJ1159+2914	179.88263	29.24556	115931+291444	0.729	13.5	-11.1	22.6	-10.8
5BZQJ2203+3145	330.81210	31.76056	220314+314538	0.295	13.4	-10.9	20.9	-11.1
5BZQJ0336+3218	54.12542	32.30806	033630+321829	1.259	12.8	-11.3	20.2	-10.5
5BZUJ1310+3220	197.61940	32.34550	131028+322044	0.997	13.1	-10.8	22.2	-10.8
5BZQJ1613+3412	243.42084	34.21333	161341+341247	1.397	12.3	-11.5	21.7	-11.6
5BZQJ1635+3808	248.81454	38.13458	163515+380804	1.814	12.5	-11.1	21.7	-10.3
5BZQJ1130+3815	172.72198	38.25514	113053+381519	1.733	12.3	-11.7	22.6	-11.6
5BZQJ0927+3902	141.76254	39.03914	092703+390220	0.695	12.1	-11.2	-	-
5BZQJ0555+3948	88.87837	39.81366	055530+394848	2.365	12.0	-11.7	20.8	-10.9
5BZBJ1653+3945	253.46750	39.76000	165352+394536	0.033	17.8	-10.2	25.2	-10.6
5BZQJ1640+3946	250.12347	39.77898	164029+394646	1.660	12.9	-11.9	22.7	-10.8
5BZQJ1642+3948	250.74506	39.81028	164258+394837	0.593	13.0	-10.6	21.7	-10.7
5BZQJ2007+4029	301.93726	40.49683	200744+402948	1.736	12.2	-11.6	-	-
5BZQJ0948+4039	147.23059	40.66239	094855+403944	1.249	12.3	-11.8	20.8	-11.2
5BZUJ0319+4130	* 49.95042	41.51167	031948+413042	0.018	13.0(?)	-10.4	23.3	-10.4
5BZBJ2202+4216	330.68042	42.27750	220243+421640	0.069	13.6	-10.0	21.3	-10.3
5BZUJ0909+4253	137.38959	42.89613	090933+425347	0.670	12.9	-11.5	20.9	-11.7
5BZQJ0646+4451	101.63346	44.85461	064632+445116	3.396	11.6	-11.8	21.8(?)	-11.5
5BZQJ0920+4441	140.24359	44.69833	092058+444153	2.190	12.5	-11.2	22.3	-10.6
5BZQJ2354+4553	358.59033	45.88445	235421+455304	1.992	12.2	-11.9	21.4	-11.7
5BZQJ0136+4751	24.24412	47.85809	013658+475129	0.859	13.3	-10.9	22.2	-10.7
5BZUJ1829+4844	277.38251	48.74628	182931+484446	0.695	13.0	-11.3	20.7	-11.1
5BZQJ1153+4931	178.35196	49.51911	115324+493109	0.334	12.9	-10.9	21.2	-11.1
5BZQJ0808+4950	122.16529	49.84347	080839+495036	1.432	12.0	-12.2	20.6	-11.7
5BZQJ0359+5057	59.87396	50.96394	035929+505750	1.512	12.1	-10.7	21.3	-10.4
5BZQJ2038+5119	309.65433	51.32018	203837+511913	1.686	12.5	-11.5	21.4	-11.0
5BZQJ1955+5131	298.92810	51.53015	195542+513149	1.214	12.7	-11.7	20.7	-11.4
5BZQJ1740+5211	265.15408	52.19528	174036+521143	1.381	13.2	-11.3	21.3	-10.8
5BZBJ1419+5423	214.94417	54.38722	141946+542315	0.153	13.7	-10.6	21.9	-11.5
5BZBJ1824+5651	276.02948	56.85042	182407+565101	0.663	13.2	-11.3	22.1	-11.0
5BZUJ0102+5824	15.69067	58.40310	010245+582411	?0.644	12.6	-11.1	21.8	-10.9
5BZQJ2022+6136	305.52783	61.61633	202206+613658	0.228	12.9	-11.2	-	-
5BZBJ0958+6533	149.69666	65.56499	095847+653354	0.367	13.4	-11.0	21.2	-11.3
5BZQJ1849+6705	282.31833	67.09403	184915+670540	0.657	13.1	-10.9	22.5	-10.6
5BZQJ0228+6721	37.20854	67.35084	022850+672101	0.523	12.8	-11.2	21.1	-11.4
5BZQJ1642+6856	250.53271	68.94437	164207+685638	0.751	12.5	-11.6	20.1(?)	-12.3
5BZBJ1806+6949	271.71124	69.82445	180650+694928	0.046	14.0	-10.6	21.7	-11.0
5BZQJ0841+7053	130.35153	70.89506	084124+705341	2.218	12.4	-11.3	20.1	-10.2
5BZBJ0721+7120	110.47208	71.34333	072153+712036	0.0	13.9	-10.3	23.3	-10.5
5BZQJ0217+7349	34.37833	73.82555	021730+734932	2.367	12.2	-11.6	20.5	-10.4
5BZQJ1927+7358	291.95209	73.96711	192748+735802	0.302	13.1	-10.8	-	-
5BZBJ2005+7752	301.37961	77.87861	200531+775243	0.342	13.2	-11.2	21.5	-11.3
5BZBJ1800+7828	270.19034	78.46778	180045+782805	0.680	13.5	-10.7	21.9	-10.9
5BZQJ1153+8058	178.30208	80.97476	115312+805829	1.250	12.6	-12.0	21.1	-11.9
5BZQJ2356+8152	359.09497	81.88118	235622+815252	1.344	12.8	-11.8	21.1	-11.5
M87	187.70592	12.39111	123049+122321	0.0042	13.0	-10.5	18.5(?)	-10.4
3C111	64.58867	38.02661	041820+380148	0.0485	13.3	-10.6	20.1	-10.0